Available online at www.sciencedirect.com
SCIENCE DIRECT®
International Journal of Solids and Structures 42 (2005) 2089–2128
INTERNATIONAL JOURNAL OF SOLIDS and STRUCTURES
www.elsevier.com/locate/ijsolstr

Compressive failure model for fiber composites by kink band initiation from obliquely aligned, shear-dislocated fiber breaks

J. Bai, S.L. Phoenix *

Department of Theoretical and Applied Mechanics, Cornell University, Ithaca, NY 14853, USA

Received 13 December 2003; received in revised form 16 August 2004
Available online 11 November 2004

Abstract

Predicting compressive failure of a unidirectional fibrous composite is a longstanding and challenging problem that we study from a new perspective. Motivated by previous modelling of tensile failure as well as experimental observations on compressive failures in single carbon fibers, we develop a new micromechanical model for the compressive failure process in unidirectional, planar composites. As the compressive load is increased, random fiber failures are assumed to occur due to statistically distributed flaws, analogous to what occurs in tension. These breaks are often shear-mode failures with slanted surfaces that induce shear dislocations, especially when they occur in small groups aligned obliquely. Our model includes interactions of dislocated and neighboring intact fibers through a system of fourth-order, differential equations governing transverse deformation, and also allows for local matrix plastic yielding and debonding from the fiber near and within the dislocation arrays. Using the Discrete Fourier Transform method, we find a 'building-block' analytical solution form, which naturally embodies local length scales of fiber microbuckling and instability. Based on the influence function, superposition approach, a computationally efficient scheme is developed to model the evolution of fiber and matrix stresses. Under increasing compressive strain the simulations show that matrix yielding and debonding crucially lead to large increases in bending strains in fibers next to small groups of obliquely aligned, dislocated breaks. From the paired locations of maximum fiber bending in flanking fibers, the triggering of an unstable kink band becomes realistic. The geometric features of the kink band, such as the fragment lengths and orientation angles, will depend on the fiber and matrix mechanical and geometric properties. In carbon fiber–polymer matrix systems our model predicts a much lower compressive failure stress than obtained from Rosen's classic microbuckling model, yielding values much closer to those observed experimentally.

Keywords: Compressive failure of composites; Dislocated fiber breaks; Kink bands

* Corresponding author. Tel.: +1 607 255 8818; fax: +1 607 255 2011.
E-mail address: slp6@cornell.edu (S.L. Phoenix).

0020-7683/$ - see front matter © 2004 Elsevier Ltd. All rights reserved.
doi:10.1016/j.ijsolstr.2004.08.011

1. Introduction

Compressive strengths of unidirectional fiber–matrix composites generally range from 20% to 60% of their tensile values. Since their rapid development, starting in the 1960s, this relative weakness has often been the limiting factor in applications of such composites, and its cause has been the subject of investigation in many works, e.g., Rosen (1965), Argon (1972), Greszczuk (1982), Budiansky (1983), Hahn and Williams (1986), Waas et al. (1990), Steif (1990a,b), Ha and Nairn (1992), Budiansky and Fleck (1993), Fleck et al. (1995), Schultheisz and Waas (1996), Waas and Schultheisz (1996), Chaudhuri et al. (1996), Vogler and Kyriakides (1999a,b), Berbinau et al. (1999) and Yerramalli and Waas (2004b). Despite this longstanding effort, compressive failure phenomena remain poorly understood. Many mechanical and geometric factors influence the threshold stress for compressive collapse, and considered together or separately, may trigger several possible failure modes as Hahn and Williams (1986) point out.

About 40 years ago, fiber microbuckling was identified as a viable failure mode and Rosen (1965) was the first to analyze this mechanism in a systematic way. Rosen drew upon the classic model of a beam on an elastic foundation and modelled the composite as an infinite array of equi-spaced, parallel bars with an elastic matrix in between. Under a compressive load, the fibers in his model displace transversely in one of two distinct periodic modes: an extension mode and a shear mode, as shown in Fig. 1. For elastic polymer matrices and fiber volume fractions less than about 30%, the extension mode of failure is predicted to dominate as adjacent fibers suddenly develop sinusoidal deformation patterns 180° out of phase. Thus, along the fiber axis the matrix between the fibers is placed in alternating transverse tension and compression. For fiber volume fractions greater than 30%, the shear mode is predicted to dominate as fibers suddenly deform transversely in phase. Thus, along the fiber axis the matrix between the fibers is placed in alternating shear in proportion to the change in local slope of the fiber center-line (over a long wave-length). Rosen (1965) theoretically derived the critical collapse stress for these two microbuckling modes in terms of fiber and matrix tensile and shear moduli, and certain geometric parameters. For the extension mode his model predicts a critical composite stress for compressive failure, $\sigma_{c,cr}$, which is

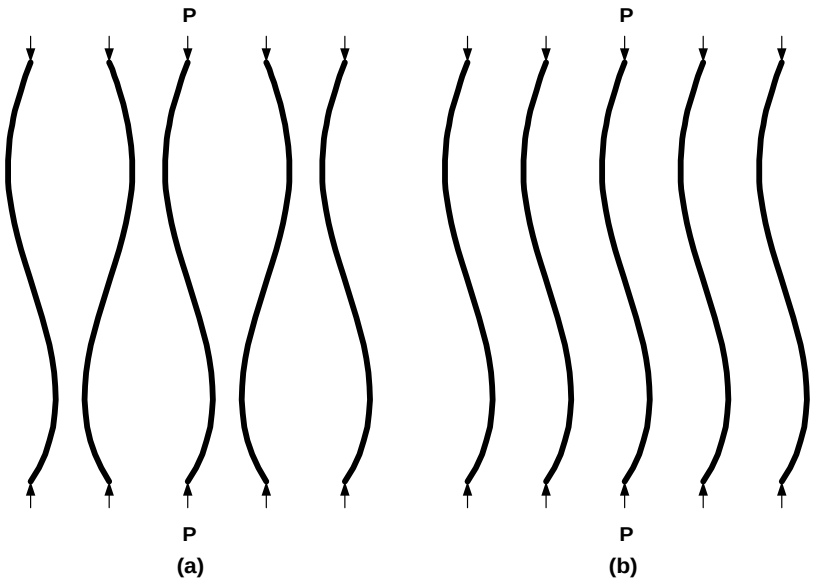

Fig. 1. Schematic of Rosen's two modes of composite failure in compression: (a) extension mode and (b) shear mode.

$$\sigma_{c,cr} \approx \sqrt{\frac{V_f^3 E_m E_f}{3(1-V_f)}}, \tag{1}$$

and for the shear mode the composite compressive failure stress is

$$\sigma_{c,cr} \approx \frac{G_m}{(1-V_f)}, \tag{2}$$

where V_f is the fiber volume fraction, E_m is the matrix Young's modulus, G_m is the matrix shear modulus and E_f is the fiber Young's modulus. In the shear mode the critical compressive strain for composite failure, $\epsilon_{c,cr}$, is

$$\epsilon_{c,cr} \approx \frac{G_m}{(1-V_f)V_f E_f}, \tag{3}$$

which is also the critical compressive strain, $\epsilon_{f,\mathrm{cr}}$, in the fiber. (Throughout the paper, compressive stresses and strains are taken as positive and tensile ones as negative.) Unfortunately, Rosen's predicted failure stresses are two to four times higher than those typically observed experimentally.

Upon noting the prevalence of distinct kink bands in compressive failure, Argon (1972) took a somewhat different approach. He developed a precursor model for kink band formation based on matrix plastic yielding and initial fiber misalignment inherited from processing the material. In his model, the critical compressive failure stress for the composite was found to be

$$\sigma_{c,cr} \approx \frac{\tau_{m,y}}{\gamma_{f,0}}, \tag{4}$$

where $\tau_{m,y}$ is the matrix yield stress in shear and $\gamma_{f,0}$ is the initial fiber misalignment angle. Subsequent research has mostly been based on various extensions of the microbuckling models of Rosen (1965) to include inelastic and misalignment effects of Argon (1972). For instance, Fleck et al. (1995) give a result which can be written as

$$\sigma_{c,cr} \approx \frac{G_m}{(1-V_f)\left(1+\frac{G_m\gamma_{f,0}}{\tau_{m,y}(1-V_f)}\right)}, \tag{5}$$

which is a variation on an earlier result by Hahn and Williams (1986). Both essentially combine the results of Rosen (1965) and Argon (1972) given above.

Other models have considered more elaborate kinds of periodic or localized fiber misalignments inherited from processing as well as matrix inelasticity. See for example Budiansky (1983), Hahn and Williams (1986), Waas et al. (1990), Steif (1990a,b), Ha and Nairn (1992), Budiansky and Fleck (1993) and Vogler and Kyriakides (1999a,b). In one variation Hahn and Williams (1986) and Berbinau et al. (1999) have examined the microbuckling phenomenon from the point of view of the equilibrium of a single fiber in a yielding matrix and undergoing bending prior to kink band formation. It was argued that a fiber could break at the point of maximum curvature (from excessive local tension or compression near the fiber surface), so the composite compressive failure strength could be related to initial waviness, the volume fraction of the fibers and the fiber failure stress in bending. In a different direction, Steif (1990a,b) proposed a model that involved the deflection of a bundle of slightly misaligned fibers until fiber breakage occurred in two planes, which brought the fibers into a kinked configuration. With kinks assumed to have experimentally observed widths, his analysis provided a reasonable connection between the fiber breaking strain and the composite compressive strength. Steif, however, pointed out the absence in his model of key but unknown factors that seem to play a key role in determining the actual kink band geometry and critical failure stress. Indeed many mechanical and geometric factors influence the threshold stress for compressive collapse, and

considered together or separately, may trigger several possible failure modes. Lee and Waas (1999) and Yerramalli and Waas (2003) point out that glass fiber composites demonstrate a simultaneous splitting/kink banding failure mode for high fiber volume fractions, which further complicates failure process interpretation.

Thus, despite all these modelling efforts, a satisfactory explanation is yet to be found for the mechanism and critical load for the onset of kink band formation. In particular, it is unclear what local fiber and matrix micromechanical features determine the critical failure stress and the experimentally observed parameter values for the resulting kink band geometry (Fig. 2), as described by kink band angle a, tilt angle b and length D of fiber fragments in the kink. Moreover, apart from the work of Waas et al. (1990), little research has been conducted on the mutual interaction of unequally deformed fibers in a multi-fiber composite system under compression. Most of the work cited above has been directed towards a single fiber or regularly deformed fiber arrays with identical, initially frozen-in, misalignment or waviness in each fiber, inherited from processing and difficult to determine prior to testing.

Behavior in compressive failure also differs with the fiber type and diameter (Yerramalli and Waas, 2004a,b). Several workers have noted the strong tendency for carbon fibers to fail first in a shear mode instead of by bending from microbuckling, which is more prevalent in glass fibers. This generates a slant failure surface and subsequent dislocation by slip (Hawthorne and Teghtsoonian, 1975; Hahn and Sohi, 1986; Oshawa et al., 1990; Boll et al., 1990; Shioya and Nakatani, 2000; Schorr, 2001; Goutianos et al., 2002, 2003). As in tensile failure, there also appears to be large variability in the local compressive fiber stress at which such failures occur (Hawthorne and Teghtsoonian, 1975; Evans and Adler, 1978; Boll et al.,

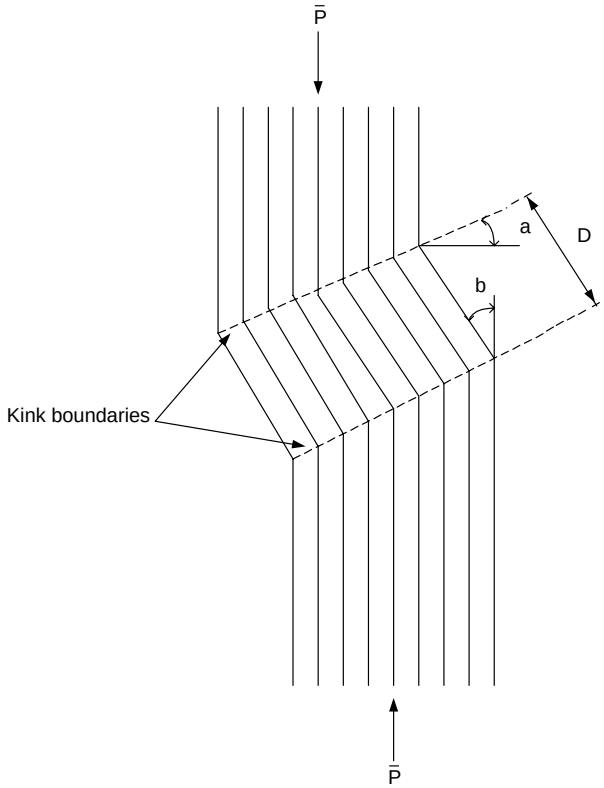

Fig. 2. Kink band geometry and notation, where a is the shear band angle, b the angle of fiber tilt and D the fiber fragment length.

Fig. 3. Compressive shear failures seen by Schorr (2001) in two single-filament-composite samples consisting of carbon fibers (Hexcel AS-4, PAN-based) in a transparent epoxy (Dow DER 331 epoxy and Dow DEH 26 curing agent): (a) sample 1 and (b) sample 2. The amount of slip and overlap was found to depend on the fiber surface treatment.

1990; Oshawa et al., 1990; Shioya and Nakatani, 2000; Schorr, 2001). In single-filament-composite experiments Schorr (2001) observed many shear failures in Hexcel PAN-based, AS-4 carbon fibers in an epoxy, as shown in Fig. 3, and presented data suggesting a Weibull distribution for fiber compressive strength with shape parameter similar to that in tension (about 7), and Evans and Adler (1978) cite a similar value. In similar single-fiber-composite experiments Boll et al. (1990) reported seeing 'first' fiber failures at stresses an order of magnitude below mean values typically seen (e.g., Shioya and Nakatani, 2000), again an indication of large variability. There is also considerable variability seen in the compressive strengths of otherwise identical coupons (e.g., see data in Hahn and Williams, 1986), often more than in tension.

1.1. Key ideas and organization of the paper

In recent experiments by Narayanan and Schadler (1999), carbon fiber breaks were reported to occur before and during kink-band formation and many had slanted failure surfaces suggesting crushing or shear failure occurs first. Thus, these authors envisioned a new failure mechanism whereby a small, slant-aligned sequence of fiber breaks develops in shear or crushing failures and triggers kink-band formation through excessive overloading of neighboring fibers to the point of bending and failure. This theme, illustrated in Fig. 4 from Garland et al. (2001), was investigated theoretically by these authors who modified a tensile failure model of Beyerlein and Phoenix (1996) to allow crushing and interpenetration at fiber failure surfaces, thus resulting in enhanced compressive overloads on neighboring fibers. However, the model, based on a system of second-order differential equations with longitudinal fiber displacements only, could not allow for transverse fiber deflections. Thus, it could not directly model fiber bending or the onset of buckling instability and kink band initiation. The goal of the present paper is to model the transverse fiber deformation directly in order to investigate the details of how a local fiber bending and buckling mechanism might occur and trigger a kink band.

Our method uses a modification of the influence function, superposition approach analogous to that in Beyerlein and Phoenix (1996) for tension and Garland et al. (2001) for compression. A key difference, however, is that modeling transverse deflection requires a fourth-order system of differential equations consistent with the models of Rosen (1965), Hahn and Williams (1986) and Waas et al. (1990), among others. We treat fibers as beams, while the matrix in between can locally undergo elastic then plastic deformation in both tension and shear. We also model the case where the matrix debonds from the fiber from excessive

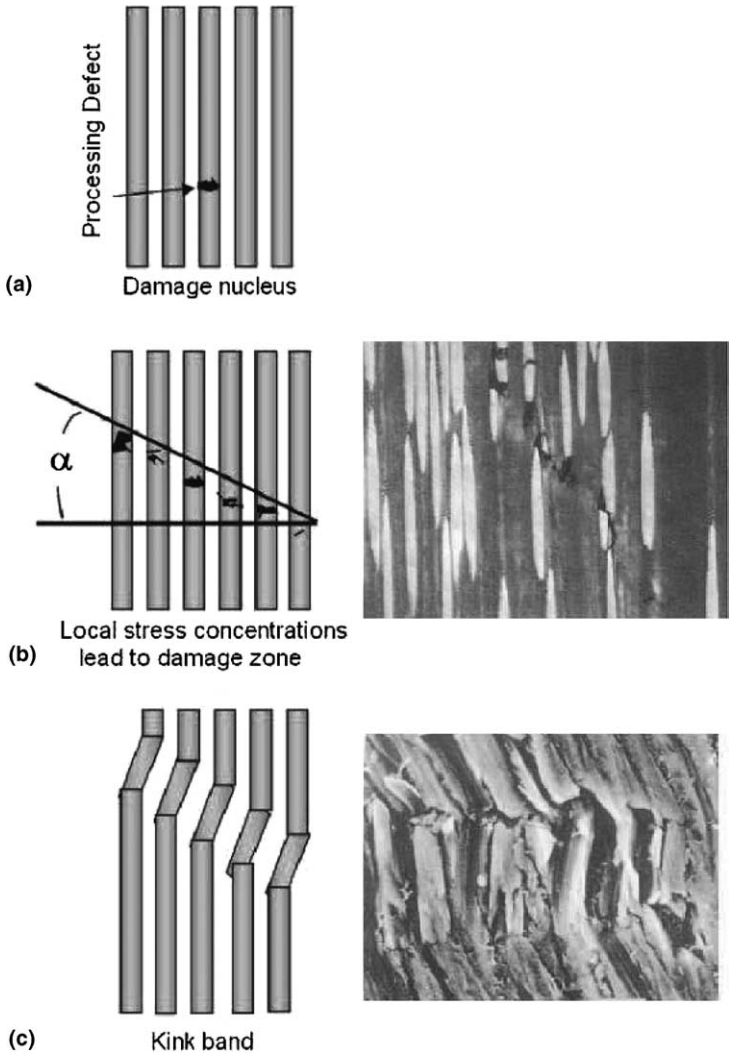

Fig. 4. Schematic of fiber failure sequence in shear triggering kink band formation. (From Garland et al., 2001).

tension or shear. Fiber matrix interactions and interface properties have long been known to be important in compressive failure. Recent experimental and modelling studies in single filament composites by Goutianos et al. (2002), Goutianos et al. (2003) further underscore this importance. Thus, the present paper appears to be the first theoretical work on the study of the actual mechanism by which a unidirectional, multi-fiber composite system containing failed fibers in shear (and some perhaps by crushing) could develop a kink band from excessive bending and failure of neighboring fibers, thus complementing the work of Garland et al. (2001).

We offer the following basic process of kink band initiation in a planar array: Upon applying a compressive load to the composite, fibers fail randomly at flaws in compression or shear and some form small oblique groups (perhaps through the sequential failure mechanism of Garland et al., 2001). Increasing the load leads to increasing slip and shear-dislocations that laterally displace neighboring intact fibers causing bending and shear disturbances. These displacement disturbances intensify as the matrix between fibers

undergoes plastic yielding in tension (or compression) or in shear. With further compressive load increases, the disturbances may become large enough to statistically generate some new shear breaks, thus increasing the size of the defect cluster. The key feature, however, is that the bending strain in each of the neighboring intact fibers, which grows with the number of obliquely aligned fiber breaks, will be high at two locations spanning the adjacent dislocation and separated by a few fiber diameters (rather than one as typically occurs in tension or shear). Eventually the compressive load is high enough for the neighboring fibers to fail at both high bending locations, thus triggering instability in the form of a well-defined kink band, whose width will be close to the distance between the peak bending stresses. Our goal is to elucidate the essential details of how a single oblique array of fiber breaks could trigger an unstable kink band with typically observed values for compressive strength and geometric parameters as in Fig. 2.

The paper is organized as follows: Section 2 describes the basic model and resulting system of fourth-order differential equations in both dimensional and non-dimensional terms, as well as the form of the solution using of Discrete Fourier Transforms. Section 3 presents three 'unit' solutions used in the influence function, superposition approach, these being solutions for a single-fiber dislocation, a matrix tensile dipole, and a matrix shear dipole, respectively. Section 4 introduces the influence function solution method for the multiple fiber dislocation problem under no matrix yielding, where the solution is a weighted sum of unit dislocation solutions. Section 5 extends this method to include plastic yielding or debonding of matrix elements, and gives the solution strategy to satisfy boundary conditions associated with the yielding or debonding matrix. Section 6 describes the general computational framework for investigating the possibility of kink band initiation from an oblique array of dislocated breaks as well as our assumptions on the induced shear loads at fiber dislocations due to the applied compressive load. Section 7 presents some case studies, and Section 8 presents a brief discussion of possible shortcomings in the model and some conclusions.

2. Model formulation

We consider an infinite planar composite lamina with an infinite number of evenly spaced, parallel fibers and loaded in the far field by compressive force $\overline{P}$ per fiber. As shown in Fig. 5, the center fiber along the x-axis is numbered $n = 0$, the fibers in the positive y direction are numbered $n = 1, 2, 3, \ldots$ and in the negative y direction, $n = -1, -2, -3, \ldots$ We number the matrix bays similarly, but with matrix bay 0 taken to lie between fiber 0 and fiber 1. Also t is the fiber spacing, i.e., the distance between the center-lines of two adjacent fibers, and d is the fiber diameter and composite thickness. Thus, the effective matrix thickness between fibers will be taken to be $t - d$. The orientation of the x–y axis is indicated and transverse fiber displacements, w_n, will be taken as positive in the y direction. To this description we will later add fiber dislocations and yielded matrix elements.

2.1. Development of system of governing differential equations

A free body diagram of an infinitesimal segment of fiber n is shown in Fig. 6. The interfacial tensile and shear traction components on the upper (right) side of the fiber element are, respectively, $\bar{\sigma}_n$ and $\bar{\tau}_n$, which are the normal and shear tractions caused by the deformation of matrix bay n between fiber n and fiber $n + 1$. (As mentioned earlier, throughout the paper, compressive stresses and strains will be taken as having positive values and tensile stresses and strains as having negative values. Also, we apply '¯' to denote dimensional load quantities and will delete it when referring to non-dimensional versions.) The tractions on the lower (left) side of the fiber are, respectively, $\bar{\sigma}_{n-1}$ and $\bar{\tau}_{n-1}$ due to the deformation of matrix bay $n - 1$ between fiber $n - 1$ and fiber n. Additionally, $\overline{Q}_n$, $\overline{M}_n$ and $\overline{P}_n$ are the shear load, bending moment and compressive force, respectively, for fiber n (as in beam theory).

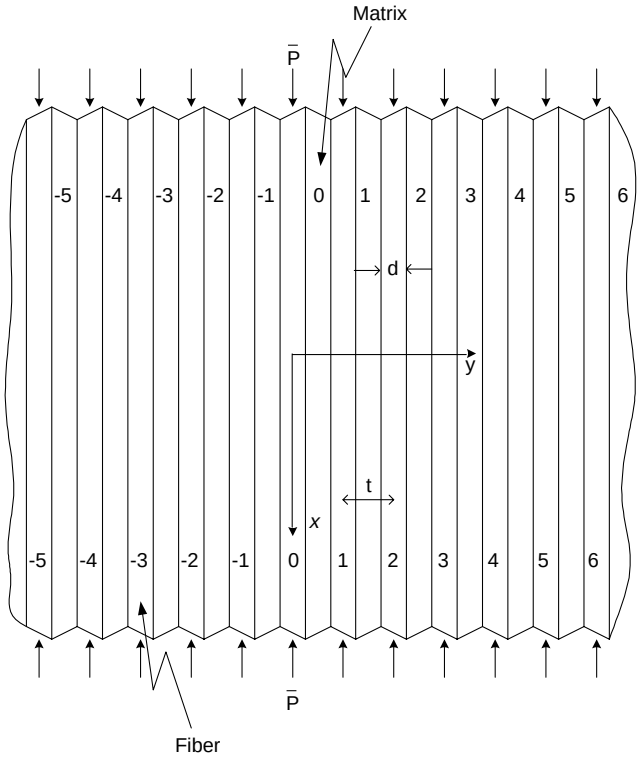

Fig. 5. Notation for a two dimensional infinite lamina subjected to a remote uniform compressive load.

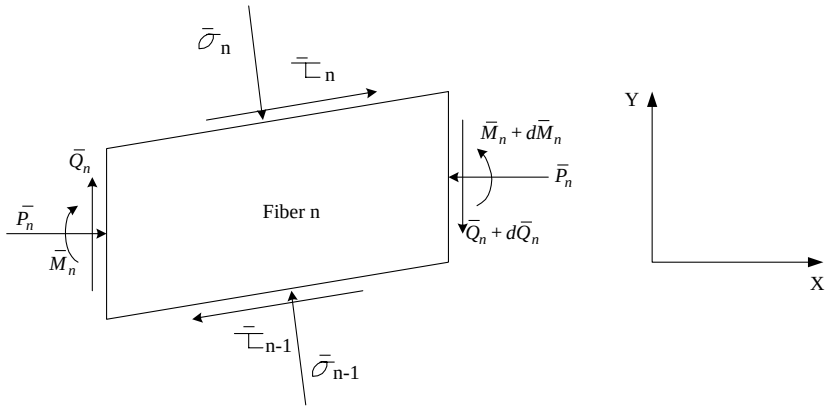

Fig. 6. Free body diagram of an infinitesimal segment of fiber n, with sign convention as indicated.

By our sign convention we assume that

$$\bar{\sigma}_n = -E_m\left(\frac{w_{n+1} - w_n}{t - d}\right) \tag{6}$$

and

$$\bar{\tau}_n = \frac{G_m}{2}\left(1+\frac{d}{t-d}\right)\left(\frac{\mathrm{d}w_n}{\mathrm{d}x}+\frac{\mathrm{d}w_{n+1}}{\mathrm{d}x}\right) \tag{7}$$

for all $-\infty < n < \infty$, where G_m and E_m are the shear modulus and Young's modulus of the matrix respectively, and w is the lateral fiber displacement. The addition of the factor $d/(t-d)$ is common in previous literature and accounts for the fiber rotation inducing a vertical displacement at fiber radius $d/2$, which enhances the matrix shear beyond what occurs by just changing the fiber slope. Note that these two equations govern the elastic matrix response, inelastic behavior being treated later.

We assume that the axial load per fiber, $\overline{P}_n$, is constant along the fibers. The equilibrium equation for loads in the lateral y direction in fiber n is

$$\frac{\mathrm{d}\overline{Q}_n}{\mathrm{d}x} = E_m\left(\frac{d}{t-d}\right)(w_{n+1}+w_{n-1}-2w_n), \tag{8}$$

and the equation balancing bending moments is

$$\frac{\mathrm{d}\overline{M}_n}{\mathrm{d}x}+\overline{P}\frac{\mathrm{d}w_n}{\mathrm{d}x} = \frac{A_f}{2}(\bar{\tau}_n+\bar{\tau}_{n-1})+\overline{Q}_n, \tag{9}$$

where A_f is the fiber cross-sectional area. (The term with A_f is easiest to appreciate for a square fiber cross-section since $(d/2)d = A_f/2$ where $d/2$ is the moment arm of the shear force per unit length and d is the lamina thickness.) Also

$$\overline{M}_n = E_f I_f \frac{\mathrm{d}^2 w_n}{\mathrm{d}x^2}, \tag{10}$$

where E_f is the fiber Young's modulus, I_f is the moment of inertia of the fiber cross-section in bending. We will take A_f and I_f to be those for a circular fiber cross-section, i.e.,

$$A_f = \pi d^2/4, \quad I_f = \pi d^4/64. \tag{11}$$

Combining the above expressions we obtain a system of fourth-order, differential equations governing the transverse deformation of the fibers, namely

$$E_f I_f \frac{\mathrm{d}^4 w_n}{\mathrm{d}x^4}+\overline{P}\frac{\mathrm{d}^2 w_n}{\mathrm{d}x^2}-\frac{B}{4}\left(\frac{\mathrm{d}^2 w_{n+1}}{\mathrm{d}x^2}+\frac{\mathrm{d}^2 w_{n-1}}{\mathrm{d}x^2}+2\frac{\mathrm{d}^2 w_n}{\mathrm{d}x^2}\right)-K(w_{n+1}+w_{n-1}-2w_n)=0, \tag{12}$$

where

$$B = G_m A_f\left(\frac{t}{t-d}\right) \tag{13}$$

and

$$K = E_m\left(\frac{d}{t-d}\right). \tag{14}$$

Note that the shear force $\overline{Q}_n$ can be written as

$$\overline{Q}_n = E_f I_f \frac{\mathrm{d}^3 w_n}{\mathrm{d}x^3}+\overline{P}\frac{\mathrm{d}w_n}{\mathrm{d}x}-\frac{B}{4}\left(\frac{\mathrm{d}w_{n+1}}{\mathrm{d}x}+\frac{\mathrm{d}w_{n-1}}{\mathrm{d}x}+2\frac{\mathrm{d}w_n}{\mathrm{d}x}\right). \tag{15}$$

2.2. Non-dimensionalization of governing equations

To simplify the presentation of results, it is convenient to non-dimensionalize the governing equations and quantities of interest using certain normalizing scales. The length scale we choose is the fiber diameter, d, whereby the transverse displacement, w_n, and axial coordinate, x, are non-dimensionalized as

$$W_n = w_n/d \tag{16}$$

and

$$\xi = x/d, \tag{17}$$

respectively. The second scale we chose is the fiber normalizing force, $E_f I_f/d^2$, and this suggests a normalizing stress, $E_f I_f/d^4$, and normalizing bending moment, $E_f I_f/d$. Applying these normalizations to Eq. (12), we obtain its non-dimensional form

$$\frac{\mathrm{d}^4 W_n}{\mathrm{d}\xi^4} + 16\epsilon_c \frac{\mathrm{d}^2 W_n}{\mathrm{d}\xi^2} - \phi\left(\frac{\mathrm{d}^2 W_{n+1}}{\mathrm{d}\xi^2} + \frac{\mathrm{d}^2 W_{n-1}}{\mathrm{d}\xi^2} + 2\frac{\mathrm{d}^2 W_n}{\mathrm{d}\xi^2}\right) - \kappa(W_{n+1} + W_{n-1} - 2W_n) = 0, \tag{18}$$

where

$$\phi = 4\frac{G_m}{E_f}\left(\frac{t}{t-d}\right), \tag{19}$$

$$\kappa = \frac{64}{\pi}\frac{E_m}{E_f} \tag{20}$$

and

$$\epsilon_c = \frac{\overline{P}}{A_f E_f}. \tag{21}$$

The normalized matrix transverse tensile (or compressive) stress, σ_n, shear stress, τ_n, fiber bending moment, M_n, fiber shear force, Q_n, and bending induced fiber strain (at the outside fiber surface), $\varepsilon_{b,n}$, are found from there dimensional counterparts above to be, respectively,

$$\sigma_n = \frac{\bar{\sigma}_n}{E_f I_f/d^4} = -\kappa(W_{n+1} - W_n), \tag{22}$$

$$\tau_n = \frac{\bar{\tau}_n}{E_f I_f/d^4} = \frac{8\phi}{\pi}\left(\frac{\mathrm{d}W_n}{\mathrm{d}\xi} + \frac{\mathrm{d}W_{n+1}}{\mathrm{d}\xi}\right), \tag{23}$$

$$M_n = \frac{\mathrm{d}^2 W_n}{\mathrm{d}\xi^2}, \tag{24}$$

$$Q_n = \frac{\mathrm{d}^3 W_n}{\mathrm{d}\xi^3} + 16\epsilon_c \frac{\mathrm{d}W_n}{\mathrm{d}\xi} - \phi\left(\frac{\mathrm{d}W_{n+1}}{\mathrm{d}\xi} + \frac{\mathrm{d}W_{n-1}}{\mathrm{d}\xi} + 2\frac{\mathrm{d}W_n}{\mathrm{d}\xi}\right) \tag{25}$$

and

$$\varepsilon_{b,n} = \frac{1}{2}\frac{\mathrm{d}^2 W_n}{\mathrm{d}\xi^2}. \tag{26}$$

We must add boundary conditions to this system of equations reflecting fiber and matrix damage in terms of fiber end loads at a given array of fiber dislocations, as well as matrix stresses after yielding or debonding. This is deferred to later sections after we have solved three 'unit' problems, which will give the overall system response to an arbitrarily located single fiber dislocation, and also to an equal and opposite force pair and a torque pair applied respectively to two adjacent fibers. These unit problems will then be used to generate influence functions used in a superposition technique to yield the fiber displacements due to fiber breaks and matrix yielding or debonding 'damage' consistent with the applied compressive load on the composite.

To generate the influence functions from the unit solutions we use a Discrete Fourier Transform framework. This transform method will first be applied to the system of differential equations and will result in unknown coefficients (in terms of the transform variable), which will be explicitly obtained for the three unit problems.

2.3. Solution structure based on Discrete Fourier Transform technique

We begin by taking a Discrete Fourier Transform of the governing system of differential equations, Eq. (18), i.e., we apply

$$V(\xi,\theta)=\sum_{n=-\infty}^{\infty} W_n(\xi)\mathrm{e}^{\mathrm{i}n\theta} \tag{27}$$

to turn the infinite set of equations into a single equation. Summing the equations in n from $-\infty$ to ∞, we obtain

$$\frac{\mathrm{d}^4V}{\mathrm{d}\xi^4}-\left(4\phi\cos^2(\theta/2)-16\epsilon_c\right)\frac{\mathrm{d}^2V}{\mathrm{d}\xi^2}+\left(4\kappa\sin^2(\theta/2)\right)V=0,\quad -\pi<\theta<\pi. \tag{28}$$

To solve for $V(\xi,\theta)$ in Eq. (28), we substitute the usual exponential form

$$V(\xi,\theta)=U(\theta)\mathrm{e}^{s\xi} \tag{29}$$

and this generates the characteristic equation

$$s^4-4\lambda(\theta)s^2+4\kappa\sin^2(\theta/2)=0, \tag{30}$$

where

$$\lambda(\theta)=\phi\cos^2(\theta/2)-4\epsilon_c. \tag{31}$$

After some manipulation, we arrive at the solution form

$$V(\xi,\theta)=\begin{cases} U_1(\theta)\mathrm{e}^{-A(\theta)|\xi|}+U_2(\theta)\mathrm{e}^{-B(\theta)|\xi|}, & -\vartheta<\theta<\vartheta,\\ \mathrm{e}^{-C(\theta)|\xi|}\{U_3(\theta)\cos[D(\theta)|\xi|]+U_4(\theta)\sin[D(\theta)|\xi|]\}, & -\pi<\theta<-\vartheta,\\ \mathrm{e}^{-C(\theta)|\xi|}\{U_3(\theta)\cos[D(\theta)|\xi|]+U_4(\theta)\sin[D(\theta)|\xi|]\}, & \vartheta<\theta<-\pi, \end{cases} \tag{32}$$

where

$$A(\theta)=\sqrt{2\lambda(\theta)+2\sqrt{\lambda^2(\theta)-\kappa\sin^2(\theta/2)}}, \tag{33}$$

$$B(\theta)=\sqrt{2\lambda(\theta)-2\sqrt{\lambda^2(\theta)-\kappa\sin^2(\theta/2)}}, \tag{34}$$

$$C(\theta) = \sqrt{|\sin(\theta/2)|\kappa^{1/2} + \lambda(\theta)}, \tag{35}$$

$$D(\theta) = \sqrt{|\sin(\theta/2)|\kappa^{1/2} - \lambda(\theta)} \tag{36}$$

and

$$\vartheta = 2\arcsin\left(\frac{\sqrt{\kappa + 4\phi(\phi - 4\epsilon_c)} - \sqrt{\kappa}}{2\phi}\right), \tag{37}$$

which is obtained from solving

$$\lambda^2(\vartheta) = \kappa\sin^2(\vartheta/2) \tag{38}$$

using Eq. (31) and standard trigonometric identities with $\lambda(\vartheta) \geqslant 0$.

Solving for $U_1(\theta)$, $U_2(\theta)$, $U_3(\theta)$ and $U_4(\theta)$ requires specific boundary conditions and this is done next in the context of the three particular unit problems. For these three cases, we can then obtain the fiber displacements from the inverse transform in the form

$$W_n(\xi) = \frac{1}{2\pi}\int_{-\pi}^{\pi} V(\xi,\theta)\mathrm{e}^{-\mathrm{i}n\theta}\,\mathrm{d}\theta. \tag{39}$$

3. Unit problems for influence function solution method

In our simulations, an adaptation of the influence function superposition technique will be an efficient way to calculate the overall fiber displacement field given an array of damage sites in terms of fiber breaks and yielded or debonded matrix elements. The general features of this approach are as follows: (i) solutions to unit problems are used to develop expressions for load transmission factors that reflect the effects of damage sites on each other, (ii) through the appropriate coordinate translations, unit solutions are used to develop expressions that represent the effects of arbitrarily located individual damage sites on the fiber displacements, (iii) unit solutions for theses individual damage sites are weighted and summed such that the combined effects of the damage sites on the fiber displacements satisfy the boundary conditions, i.e., produce the appropriate shear forces at fiber break sites and the appropriate yield or debond stresses in the matrix damage zones. In the last step, obtaining the weights involves solving a mathematical matrix equation using the load transmission factors and boundary conditions associated with the damage array.

The first unit problem is to determine the fiber displacements occurring in an infinite sheet containing a single, dislocated fiber break at the origin and with unit shear displacement as shown in Fig. 7. From this we get the response to a unit shear load applied to the dislocation, which is the key result desired. The second unit problem is to determine the displacements resulting from an equal and opposite force pair applied to the two fibers flanking matrix bay 0 at the origin and acting to push them apart, as indicated in Fig. 8. The third unit problem is to determine the displacement resulting from a moment dipole pair applied to the two fibers flanking matrix bay 0 at the origin with the same counter-clockwise sense in each and producing loads and displacements in the sheet, as shown in Fig. 9. In all three unit problems, the applied load at infinity is ϵ_c. These unit problems are treated next.

3.1. Single fiber dislocation problem

We consider a single fiber break at $\xi = 0$ in fiber $n = 0$ in an infinite planar composite, and in the first calculation assume that the upper and lower ends are moved apart a unit distance to form a unit dislocation,

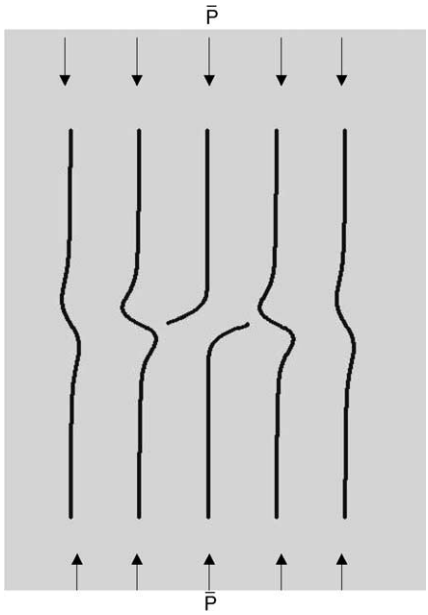

Fig. 7. Schematic of a single fiber dislocation in a two dimensional infinite lamina subjected to a remote uniform compressive load.

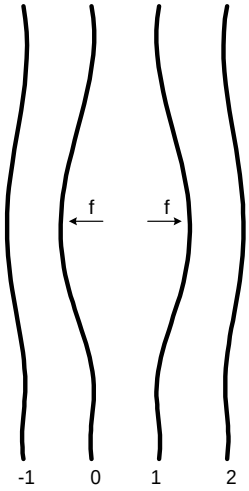

Fig. 8. Schematic showing the matrix tensile dipole problem.

as shown (exaggerated) in Fig. 7. We let $\widetilde{W}_{d,n}(\xi)$ be the unit solution to this dislocation problem, i.e., the displacement of fiber n at position ξ. Thus, we have the following boundary conditions:

$$\widetilde{W}_{d,0}(0^+) = 1/2, \tag{40}$$

$$\widetilde{W}_{d,0}(0^-) = -1/2, \tag{41}$$

$$\widetilde{W}_{d,n}(0) = 0, \quad n \geqslant 1, \ n \leqslant -1 \tag{42}$$

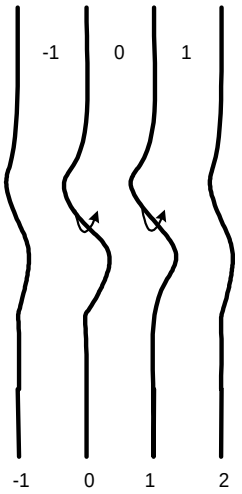

Fig. 9. Schematic showing the shear dipole problem.

and

$$\left.\frac{\mathrm{d}^2\widetilde{W}_{d,n}}{\mathrm{d}\xi^2}\right|_{\xi=0} = 0, \quad -\infty < n < \infty. \tag{43}$$

These boundary conditions reflect the facts that the displacements of the neighboring intact fibers at $\xi = 0$ are all zero since the deformation pattern is antisymmetric and the second derivatives of displacements (moments $M_n(0)$) are zero there as well.

Applying the Discrete Fourier Transform, Eq. (27), we obtain the corresponding transformed boundary conditions

$$\widetilde{V}_d(0^+, \theta) = 1/2, \tag{44}$$

$$\widetilde{V}_d(0^-, \theta) = -1/2 \tag{45}$$

and

$$\left.\frac{\mathrm{d}^2\widetilde{V}_d(\xi,\theta)}{\mathrm{d}\xi^2}\right|_{\xi=0} = 0. \tag{46}$$

After a lengthy derivation, including determining from these boundary conditions the unknown quantities $U_1(\theta)$ to $U_4(\theta)$ in Eq. (32), and combining the two cases $\xi > 0$ and $\xi < 0$, we obtain from Eq. (32) an expression for the normalized fiber displacements, which is

$$\begin{aligned}\widetilde{W}_{d,n}(\xi) = \mathrm{sign}(\xi)\Bigg\{&\frac{1}{2\pi}\int_0^{\vartheta} \frac{\mathrm{e}^{-A(\theta)|\xi|}B^2(\theta) - \mathrm{e}^{-B(\theta)|\xi|}A^2(\theta)}{B^2(\theta) - A^2(\theta)}\cos(n\theta)\,\mathrm{d}\theta \\ &+\frac{1}{2\pi}\int_{\vartheta}^{\pi} \mathrm{e}^{-C(\theta)|\xi|}\left(\cos[D(\theta)|\xi|] + \frac{C^2(\theta) - D^2(\theta)}{2C(\theta)D(\theta)}\sin[D(\theta)|\xi|]\right)\cos(n\theta)\,\mathrm{d}\theta\Bigg\}\end{aligned} \tag{47}$$

for $-\infty < n < \infty$, and where $A(\theta)$, $B(\theta)$, $C(\theta)$, $D(\theta)$ and ϑ were given, respectively, by Eqs. (33)–(37), and depend on ϵ_c.

Next we determine $\widetilde{S}_d$, the normalized shear force, $Q_0(0)$ occurring at the unit dislocation, i.e., at $\xi = 0$ and $n = 0$. From Eqs. (25) and (47) we obtain

$$\begin{aligned}\widetilde{S}_d &= \left\{ \frac{\mathrm{d}^3 \widetilde{W}_{d,0}}{\mathrm{d}\xi^3} - \phi\left(2\frac{\mathrm{d}\widetilde{W}_{d,1}}{\mathrm{d}\xi} + 2\frac{\mathrm{d}\widetilde{W}_{d,0}}{\mathrm{d}\xi} \right) + 16\epsilon_c \frac{\mathrm{d}\widetilde{W}_{d,0}}{\mathrm{d}\xi} \right\}\Bigg|_{\xi=0} \\ &= \frac{1}{2\pi}\left\{ \int_0^{\vartheta} \frac{A^2(\theta)B^2(\theta)}{A(\theta)+B(\theta)}\,\mathrm{d}\theta + \frac{1}{2}\int_{\vartheta}^{\pi} \frac{\left(C^2(\theta)+D^2(\theta)\right)^2}{C(\theta)}\,\mathrm{d}\theta \right. \\ &\quad + \phi\left(\int_0^{\vartheta} \frac{A(\theta)B(\theta)}{A(\theta)+B(\theta)}(2\cos(\theta)+2)\,\mathrm{d}\theta + \frac{1}{2}\int_{\vartheta}^{\pi} \frac{C^2(\theta)+D^2(\theta)}{C(\theta)}(2\cos(\theta)+2)\,\mathrm{d}\theta \right) \\ &\quad \left. -16\epsilon_c\left(\int_0^{\vartheta} \frac{A(\theta)B(\theta)}{A(\theta)+B(\theta)}\,\mathrm{d}\theta + \frac{1}{2}\int_{\vartheta}^{\pi} \frac{C^2(\theta)+D^2(\theta)}{C(\theta)}\,\mathrm{d}\theta \right) \right\}. \end{aligned} \tag{48}$$

This allows us to determine the key quantity, $W_{d,n}(\xi)$, which is the fiber displacement solution for a unit normalized shear force pair of magnitude $\widetilde{S}_d = 1$ applied to the dislocation tending to separate it in shear. This is easily found since we know $\widetilde{S}_d$, induced on the dislocation ends due to a unit relative displacement, and dividing Eq. (47) by $\widetilde{S}_d$ gives us

$$W_{d,n}(\xi) = \frac{\widetilde{W}_{d,n}(\xi)}{\widetilde{S}_d}. \tag{49}$$

3.2. Matrix tensile dipole problem

The solution to the matrix tensile dipole problem will allow us to approximate fiber displacements due to a matrix element with special tensile or compressive stresses acting over its length. This solution, appropriately weighted, will allow us to determine matrix stress corrections to what would be calculated from the relative fiber displacements under purely elastic matrix assumptions, as will be needed in the cases of matrix yielding or debonding.

The unit matrix tensile dipole problem can be thought of as involving two unit forces, $-f$ and f applied transversely to fibers 0 and 1 flanking matrix bay 0 at the origin $\xi = 0$. These produce fiber displacements as shown in Fig. 8. The application of these forces is reflected as jumps in internal fiber shear forces through jumps in the third derivative of displacements. These forces induce local tensile stresses in matrix bay 0. We let $W_{mt,n}(\xi)$ be the fiber displacements due to application of the unit separation force in fibers 0 and 1 at $\xi = 0$. From symmetry considerations, the corresponding boundary conditions are

$$\left.\frac{\mathrm{d}W_{mt,n}}{\mathrm{d}\xi}\right|_{\xi=0} = 0, \quad -\infty < n < \infty, \tag{50}$$

$$\left.\frac{\mathrm{d}^3 W_{mt,n}}{\mathrm{d}\xi^3}\right|_{\xi=0^+} = -\frac{1}{2}, \quad n = 0, \tag{51}$$

$$\left.\frac{\mathrm{d}^3 W_{mt,n}}{\mathrm{d}\xi^3}\right|_{\xi=0^-} = +\frac{1}{2}, \quad n = 0, \tag{52}$$

$$\left.\frac{\mathrm{d}^3 W_{mt,n}}{\mathrm{d}\xi^3}\right|_{\xi=0^+} = +\frac{1}{2}, \quad n = 1, \tag{53}$$

$$\left.\frac{\mathrm{d}^3 W_{mt,n}}{\mathrm{d}\xi^3}\right|_{\xi=0^-} = -\frac{1}{2}, \quad n = 1 \tag{54}$$

and

$$\left.\frac{\mathrm{d}^3 W_{mt,n}}{\mathrm{d}\xi^3}\right|_{\xi=0} = 0, \quad n \neq 0, 1. \tag{55}$$

Upon applying Discrete Fourier Transformation, the boundary conditions transform as follows: For $\xi > 0$, we have

$$\left.\frac{\mathrm{d}V_{mt}(\xi,\theta)}{\mathrm{d}\xi}\right|_{\xi=0} = 0, \tag{56}$$

and

$$\left.\frac{\mathrm{d}^3 V_{mt}(\xi,\theta)}{\mathrm{d}\xi^3}\right|_{\xi=0^+} = -\frac{1}{2}\left[1 - \mathrm{e}^{\mathrm{i}\theta}\right], \tag{57}$$

and for $\xi < 0$, we have

$$\left.\frac{\mathrm{d}V_{mt}(\xi,\theta)}{\mathrm{d}\xi}\right|_{\xi=0} = 0 \tag{58}$$

and

$$\left.\frac{\mathrm{d}^3 V_{mt}(\xi,\theta)}{\mathrm{d}\xi^3}\right|_{\xi=0^-} = \frac{1}{2}[1 - \mathrm{e}^{\mathrm{i}\theta}]. \tag{59}$$

From a lengthy derivation, including determining from these boundary conditions the unknown quantities $U_1(\theta)$ to $U_4(\theta)$ in Eq. (32), we obtain from Eq. (32) an expression for the normalized fiber displacements, which is

$$\begin{aligned} W_{mt,n}(\xi) = {} & \frac{1}{2\pi}\int_0^{\vartheta} \frac{A(\theta)\mathrm{e}^{-B(\theta)|\xi|} - B(\theta)\mathrm{e}^{-A(\theta)|\xi|}}{A(\theta)B(\theta)[B^2(\theta) - A^2(\theta)]}(\cos[n\theta] - \cos[(n-1)\theta])\,\mathrm{d}\theta \\ & - \frac{1}{4\pi}\int_{\vartheta}^{\pi} \frac{D(\theta)\cos[D(\theta)|\xi|] + C(\theta)\sin[D(\theta)|\xi|]}{C(\theta)D(\theta)[C^2(\theta) + D^2(\theta)]}\mathrm{e}^{-C(\theta)|\xi|}(\cos[n\theta] - \cos[(n-1)\theta])\,\mathrm{d}\theta \end{aligned} \tag{60}$$

for $-\infty < n < \infty$ where again $A(\theta)$, $B(\theta)$, $C(\theta)$, $D(\theta)$ and ϑ are given, respectively, by Eqs. (33)–(37).

3.3. Matrix shear dipole problem

The solution to the matrix shear dipole problem will allow us to approximate fiber displacement profiles due to a matrix element that has shear stresses acting over its length that differ from what would be calculated from the local fiber slopes under elastic matrix assumptions. This will be the case in matrix shear yielding or debonding, and the solution, appropriately weighted, will allow us to develop compensating shear stresses in the matrix element.

The matrix shear dipole problem involves two unit counterclockwise moments applied to consecutive fibers 0 and 1 flanking matrix bay 0 at the origin $\xi = 0$. These produce fiber distortions in the lamina sheet as shown in Fig. 9. The applied moments are reflected as negative unit jumps in curvature, i.e., in second derivatives of displacements as ξ passes through 0, and they generate positive shear stresses in matrix bay 0.

We let $W_{ms,n}(\xi)$ be the induced fiber displacements. From antisymmetry conditions the corresponding boundary conditions are thus

$$\begin{aligned}
&W_{ms,n}(0) = 0, \quad -\infty < n < \infty \\
&\left.\frac{\mathrm{d}^2 W_{ms,n}}{\mathrm{d}\xi^2}\right|_{\xi=0^+} = -\frac{1}{2}, \quad n = 0, \\
&\left.\frac{\mathrm{d}^2 W_{ms,n}}{\mathrm{d}\xi^2}\right|_{\xi=0^-} = \frac{1}{2}, \quad n = 0, \\
&\left.\frac{\mathrm{d}^2 W_{ms,n}}{\mathrm{d}\xi^2}\right|_{\xi=0^+} = -\frac{1}{2}, \quad n = 1, \\
&\left.\frac{\mathrm{d}^2 W_{ms,n}}{\mathrm{d}\xi^2}\right|_{\xi=0^-} = \frac{1}{2}, \quad n = 1
\end{aligned} \tag{61}$$

and

$$\left.\frac{\mathrm{d}^2 W_{ms,n}}{\mathrm{d}\xi^2}\right|_{\xi=0} = 0, \quad n \neq 0, 1, \ -\infty < n < \infty.$$

The last condition applies because the displacements are antisymmetric. Applying the Discrete Fourier Transform these boundary conditions become

$$\begin{aligned}
&V_{ms}(0,\theta) = 0, \\
&\left.\frac{\mathrm{d}^2 V_{ms}(\xi,\theta)}{\mathrm{d}\xi^2}\right|_{\xi=0^+} = -\frac{1}{2}\left[1 + \mathrm{e}^{\mathrm{i}\theta}\right]
\end{aligned} \tag{62}$$

and

$$\left.\frac{\mathrm{d}^2 V_{ms}(\xi,\theta)}{\mathrm{d}\xi^2}\right|_{\xi=0^-} = \frac{1}{2}\left[1 + \mathrm{e}^{\mathrm{i}\theta}\right].$$

After a lengthy derivation, including determining from the boundary conditions above the unknown quantities $U_1(\theta)$ to $U_4(\theta)$ in Eq. (32), we obtain from Eq. (32) an expression for the normalized fiber displacements, which is

$$\begin{aligned}
W_{ms,n}(\xi) = \operatorname{sign}(\xi)\Bigg\{&\frac{1}{2\pi}\int_0^{\vartheta} \frac{\mathrm{e}^{-B(\theta)|\xi|} - \mathrm{e}^{-A(\theta)|\xi|}}{A^2(\theta) - B^2(\theta)}\left(\cos[n\theta] + \cos[(n-1)\theta]\right)\mathrm{d}\theta \\
&+ \frac{1}{4\pi}\int_{\vartheta}^{\pi} \frac{\sin[D(\theta)|\xi|]}{C(\theta)D(\theta)}\mathrm{e}^{-C(\theta)|\xi|}\left(\cos[n\theta] + \cos[(n-1)\theta]\right)\mathrm{d}\theta\Bigg\}
\end{aligned} \tag{63}$$

for $-\infty < n < \infty$, and where again $A(\theta)$, $B(\theta)$, $C(\theta)$, $D(\theta)$ and ϑ were given, respectively, by Eqs. (33)–(37).

From the above displacement results can be calculated associated fiber forces and bending moments as well as matrix tensile or compressive stresses and shear stresses using Eqs. (25), (24), (22), (23) and (26), respectively.

4. Influence function solution method for multiple dislocation problem with no matrix yielding

To illustrate the approach formally, we first consider calculation of the fiber displacement field in an infinite lamina due to N fiber dislocations for the case where the matrix material is purely elastic, i.e., does not yield or debond. Fig. 10 shows an array of four dislocations ($N = 4$) in consecutive fibers and lying on an oblique plane at angle α with respect to a plane transverse to the fiber axis, as will be of interest later. Also shown is a grid of small characteristic spacing, q, where fiber and matrix elements will later have length $2q$. For computational purposes, dislocations are placed at grid points and for graphing purposes stresses and displacements are typically computed at all grid points over an area where significant deformation occurs.

To calculate the overall fiber displacements, W_n, the first analytical step is to shift the single fiber dislocation solution to apply to the actual dislocation positions. Since the fiber dislocation unit solution is translational invariant, the solution for an arbitrarily located fiber dislocation (n_i, ξ_i) is simply obtained by replacing (n, ξ) in Eq. (47) by $(n - n_i, \xi - \xi_i)$. Using superposition we can then express the overall displacements of the fibers as the weighted sum

$$W_n(\xi) = \sum_{i=1}^{N} K_{d,i} W_{d,n-n_i}(\xi - \xi_i), \tag{64}$$

where $K_{d,i}$ is a suitable weighting coefficient for dislocation i and $W_{d,n-n_i}(\xi - \xi_i)$ is given by Eq. (49) for a unit dislocation at the origin but appropriately shifted to dislocation i, as just mentioned.

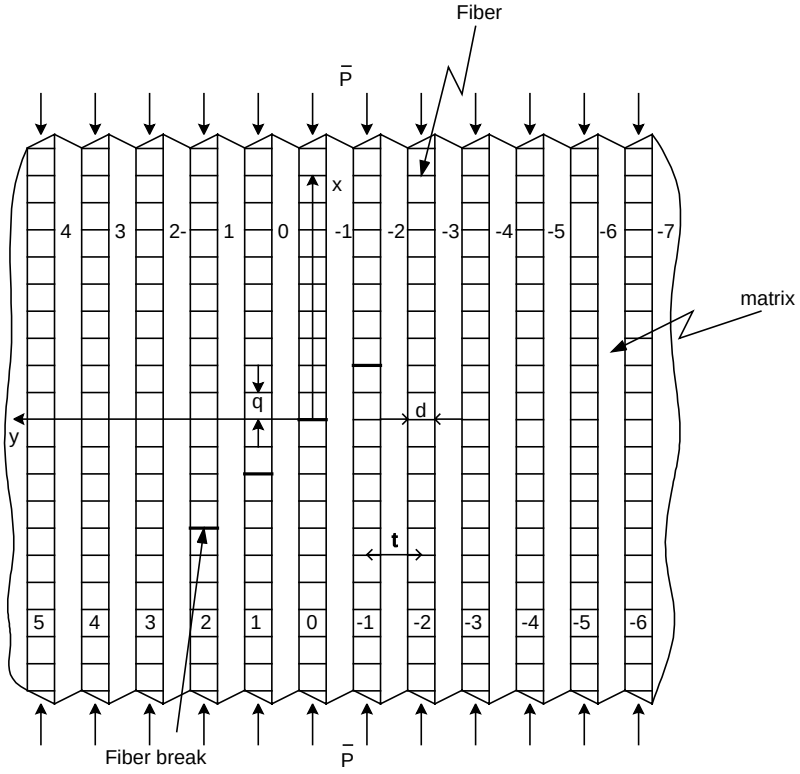

Fig. 10. Two dimensional lamina with $N = 4$ dislocations lying on an oblique plane with angle α. Discretized fiber and matrix elements (not outlined) have length $2q$, where q is the grid spacing used in numerical calculations.

The method to determine the weights, $K_{d,i}$, is as follows: From the shifted solution, $W_{d,n-n_i}(\xi - \xi_i)$, we first generate the load transmission factor, $\Lambda_{k,i}$, which is the shear load transmitted onto the fiber at the position of dislocation k at (ξ_k, n_k) due to a unit shear load acting on dislocation i at (ξ_i, n_i). This factor is calculated from Eqs. (49) and (25) and is given in the Appendix as Eq. (A.1). Next we note that the total contributions coming from all N fiber dislocations at the position of a given dislocation (including its self-contribution) must be such that the normalized shear force pair applied to the dislocation ends is S, whose prescribed value is described in more detail in Section 5. In view of Eq. (64) this leads to a system of equations for the weights $K_{d,i}$, which can be put in the matrix form

$$\begin{bmatrix} S \\ \vdots \\ S \end{bmatrix} = \begin{bmatrix} \Lambda_{1,1} & \cdots & \Lambda_{1,N} \\ \vdots & \ddots & \vdots \\ \Lambda_{N,1} & \cdots & \Lambda_{N,N} \end{bmatrix} \begin{bmatrix} K_{d,1} \\ \vdots \\ K_{d,N} \end{bmatrix}. \tag{65}$$

The load transmission factors $\Lambda_{k,i}$ are calculated by numerical integration of Eq. (A.1) for dislocation positions such as are shown in the grid in Fig. 10. This matrix equation can then be solved to yield the appropriate K-weights for use in Eq. (64).

Once the displacements, Eq. (64) are known for all the fibers, we can find the maximum bending strains in the fibers and the maximum tensile or compressive stresses and shear stresses that develop in the matrix using Eqs. (26), (22) and (23), respectively. These are calculated at grid points such as in Fig. 10 as is done in Section 7.

5. Solution method for multiple dislocation problem including yielded matrix elements

Ultimately, as the applied compressive load is increased on the composite, the matrix will yield and extensive preliminary calculations have shown that this typically occurs in matrix bays as shown in Fig. 11, where in some regions shear dominates, whereas in others, transverse tension or compression dominates. Since the mathematical solutions above assume an elastic, non-yielding matrix, we need a mathematical device to model the deviations that occur when the matrix yields plastically, and thus, cannot support any additional stress (in transverse tension, compression or shear) despite the fact that the fiber relative displacements and slopes may continue to increase. In essence, we approximately null out the excess matrix stress associated with the 'virtual' elastic solution by applying either a tension dipole (with negative coefficient in the case of compression) or a moment pair of suitable magnitude and sign and flanking the centers of suitably small matrix elements in the matrix yield region (i.e., small relative to characteristic lengths of fiber stress variation coming from buckling effects). See Fig. 10 for the grid used in the model, with spacing q and where fiber and matrix elements have length $2q$ (matrix elements not shown for clarity but are to the right of corresponding fiber elements). In other words, what acts on the fibers in a matrix yield region is a compensating discrete transverse dipole force distribution or a compensating discrete moment distribution superimposed on the 'virtual' elastic matrix response so that in total the result is virtually the same as what would have occurred if the matrix had actually yielded. The accuracy in this approximation depends on the lengths of the matrix elements, $2q$, compared to the local characteristic lengths of fiber bending and buckling reflected primarily in the exponentials in the unit solutions in Section 3.

The solution technique, thus, parallels that in Beyerlein and Phoenix (1996). Once again it is an influence function superposition involving the fiber dislocation unit solution (with unit shear load), the matrix tensile dipole unit solution and the shear dipole unit solution whereby weighting constants for the superposed and appropriately translated unit solutions are adjusted to satisfy the specified boundary conditions on the dislocations and yielded (or later debonded) matrix bays.

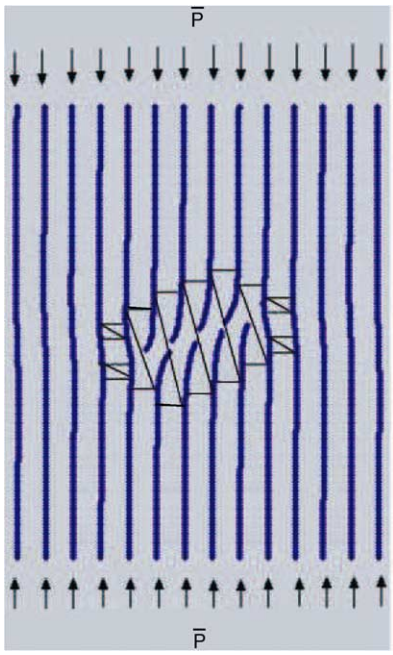

Fig. 11. Schematic showing typical yield zones in a two dimensional infinite lamina subjected to a remote uniform compressive load. The four breaks are on a slant plane at an angle α relative to the plane perpendicular to the fiber axis.

With respect to the boundary conditions (boundary loads of the damaged areas), the normalized shear force on each dislocation end is maintained at a prescribed value S (defined shortly), the normalized tension or compression force in all such yielding matrix elements is set to $2q\sigma_Y$ in absolute value, and the normalized shear force in all such shear yielding matrix elements (which is corrected for yielding by using shear dipoles) is set to $2q\tau_Y$ in absolute value, where σ_Y is the magnitude of the normalized tensile yield stress, τ_Y is the magnitude of the normalized shear yield stress. Also, these stresses are positive or negative depending on the senses of relative fiber displacements or slopes. Elsewhere in the matrix, the normal or shear stresses should be below the respective yield thresholds, and at the boundaries of the matrix yield zones, these stresses should be right at the threshold. These boundary positions must be determined using iteration, which is a time consuming aspect of the calculation. Each one of the above forces, either at a dislocation or at a yielded matrix element, will be equal to a weighted sum of the loads transmitted from the fiber dislocations and all the yielded matrix elements (including self-transmission). Therefore, it is crucial to determine the load transmission factors between two dislocations (already obtained), between a dislocation and a yielded matrix element (normal or shear) and between two yielded matrix elements (normal or shear). In all, there are nine possibilities.

The yielding criterion we have defined is oversimplified perhaps in that we have neglected coupling of shear with tension or compression in defining plastic limit values, as would occur under a Tresca yield criterion, for instance. Also, when the matrix yields, its volume tends to be preserved, which is not an issue in plane stress-like conditions as we are assuming, but may become an issue in plane strain or 3D conditions. Thus, the type of yielding we consider is approximately that of having one principal stress (through the thickness) taken as zero, and the longitudinal strain taken as negligibly small. Using Mohr's circle one can see that yielding in shear and tension or compression can coexist with the effective limit values for each somewhat reduced. What we later find, however, is that certain regions emerge where either yielding in

shear dominates or yielding in tension or compression dominates and what occurs in these regions dominates the behavior. In other words, the effects on overall behavior tend to be negligible from the small overlap regions where details of the yield criterion might be important.

5.1. Load transmission factors involving matrix element yielding

The first group of three load transmission factors involves load transmission from a shear-loaded dislocation to other dislocation or matrix element yield sites. The first is $\Lambda_{k,i}$, which was the shear load transmitted onto the fiber at the position of dislocation k at (ξ_k, n_k) due to a unit shear load acting on dislocation i at (ξ_i, n_i). This was determined earlier and is given in the Appendix by Eq. (A.1). The second is $\Omega_{k,i}$, which is defined as the effective normalized tensile force transmitted onto matrix element k due to the unit shear force acting on fiber dislocation i. This is obtained from the fiber dislocation unit solution, Eq. (49), and the definition of the normalized shear stress, Eq. (22) and is given in the Appendix by Eq. (A.2). The third is $\Gamma_{k,i}$, which is the effective induced moment dipole transmitted onto matrix element k, due to a unit shear force acting on fiber dislocation i. This is calculated from Eqs. (49) and (23) and is given in the Appendix by Eq. (A.3).

The second group of three load transmission factors involve load transmission from a tension dipole imposed at a matrix element to other dislocation or matrix element yield sites. The first is $\Phi^{(t)}_{j,k}$, which is the proportion of shear load transmitted onto the fiber at dislocation j due to a unit tension force dipole imposed at matrix element k at its center, where its length is $2q$. This is obtained using Eq. (60) and the definition of normalized fiber shear force, Eq. (25), and is given in the Appendix by Eq. (A.4). The second is $\Pi^{(t)}_{l,k}$, which is the effective matrix tensile force on matrix element l due to a unit matrix force dipole imposed at the center of matrix element k. This is obtained from Eqs. (22) and (60) and multiplying by the matrix element length $2q$, and is given in the Appendix by Eq. (A.5). The third is $\Psi^{(t)}_{l,k}$, which is the effective induced shear force pair acting on matrix element l due to a unit tension force dipole imposed at matrix k. This is obtained from Eqs. (60) and (23), and is given in the Appendix by Eq. (A.6).

The final group of three load transmission factors involve load transmission from a shear (moment) dipole imposed at a matrix element to other dislocation or matrix element yield sites. The first is $\Phi^{(s)}_{j,l}$, which is the proportion of shear load transmitted onto the fiber at dislocation j due to a unit moment dipole imposed at matrix element l. This is obtained using Eqs. (63) and (25), and is given in the Appendix by Eq. (A.7). The second is $\Pi^{(s)}_{m,r}$, which is the effective force dipole on matrix element m undergoing tension induced yielding by a unit moment dipole imposed at the location of matrix element r. This is obtained from Eqs. (63) and (22), and is given in the Appendix by Eq. (A.8). The third is $\Psi^{(s)}_{g,k}$, which is the effective moment dipole on matrix element g, due to a unit moment dipole imposed on matrix element k. This is obtained from Eqs. (63) and (23), and is given in the Appendix by Eq. (A.9).

5.2. Form of solution and solving for influence weights under boundary conditions for dislocation loads and matrix element yielding

To obtain the displacements for a given state of damage in terms of fiber dislocations and regions of matrix yielding, the calculation involves superposition of unit solutions in a manner analogous to that described in Section 4. The displacement, W_n, of fiber n at any axial distance ξ is the weighted sum of the influences of all the fiber dislocations and yielded matrix elements in the lamina, i.e.,

$$W_n(\xi) = \sum_{i=1}^{N} K_{d,i} W_{d,n-n_i}(\xi - \xi_i) + \sum_{j=1}^{s} K_{mt,j} W_{mt,n-n_j}(\xi - \xi_j) + \sum_{k=1}^{r} K_{ms,k} W_{ms,n-n_k}(\xi - \xi_k), \tag{66}$$

where $W_{d,n-n_i}(\xi-\xi_i)$, given by Eq. (49), is the displacement of fiber n due to the unit shear force on the fiber dislocation at location (ξ_i,n_i), $W_{mt,n-n_i}(\xi-\xi_i)$, given by Eq. (60), is the displacement of fiber n due to a tensile or compressive force *correction* for the yielded matrix element centered at location (ξ_j,n_j), and $W_{ms,n-n_k}(\xi-\xi_k)$, given by Eq. (63), is the displacement of fiber n due to a shear moment dipole *correction* for the yielded matrix element centered at location (ξ_k,n_k). Also $K_{d,i}$, $K_{mt,j}$, and $K_{ms,k}$ are the respective weights for the unit solutions.

The weights $K_{d,i}$ are obtained under the boundary conditions that there exists a shear force, S, on the ends of each fiber dislocation. Their role is the same as in Section 4 and a formula for S will be given shortly in terms of the applied strain ϵ_c and obliquity angle α for the N dislocation array.

The weights $K_{mt,j}$ are obtained such that the correct tensile or compressive stress appears in each yielded matrix element, which is represented (approximately) in terms of having the equivalent correct force dipoles of absolute magnitude $2q\sigma_Y$ and correct signs acting on the fibers flanking each yielded matrix element. In other words, the $K_{mt,j}$ determine the difference in normal force between what a yielded matrix element actually exerts and what it would exert on the flanking fibers if it were deforming elastically under the same relative fiber displacement. As its tensile or compressive stress goes beyond yielding, the magnitude of $K_{mt,j}$ increases from zero, and a compensating stress, opposite in sign to the elastically calculated stress, is imposed to reduce it in magnitude from the elastically determined value to the value appropriate to yielding.

By similar arguments the weights $K_{ms,k}$ are obtained such that the correct shear stresses appear in yielded matrix elements, which is represented (approximately) in terms of having the equivalent correct shear (moment) dipole of absolute magnitude $2q(\pi/8)\tau_Y$ acting on the fibers flanking each shear yielding matrix element, and with the appropriate signs depending on the direction of yielding.

Thus if there are N dislocated fiber breaks, s matrix elements yielding in tension or compression, and r matrix elements in shear yielding, a system of $N+s+r$ equations must be solved for the N weights, $K_{d,i}$, the s weights, $K_{mt,i}$, and the r weights, $K_{ms,i}$, respectively. From Eqs. (22), (23), (25) and (24) we obtain the following matrix equation to solve for these weights:

$$\begin{bmatrix} \mathbf{S} \\ 2q\boldsymbol{\sigma}_Y \\ 2q\left(\frac{\pi}{8}\right)\boldsymbol{\tau}_Y \end{bmatrix} = \begin{bmatrix} \boldsymbol{\Lambda} & \boldsymbol{\Phi}^{(t)} & \boldsymbol{\Phi}^{(s)} \\ \boldsymbol{\Omega} & \boldsymbol{\Pi}^{(t)} & \boldsymbol{\Pi}^{(s)} \\ \boldsymbol{\Gamma} & \boldsymbol{\Psi}^{(t)} & \boldsymbol{\Psi}^{(s)} \end{bmatrix} \begin{bmatrix} \mathbf{K}_d \\ \mathbf{K}_{mt} \\ \mathbf{K}_{ms} \end{bmatrix}. \tag{67}$$

In this matrix equation, $\mathbf{S}$ and $\mathbf{K}_d$ are both N-dimensional vectors, $\boldsymbol{\sigma}_Y$ and $\mathbf{K}_{mt}$ are s-dimensional vectors, and $\boldsymbol{\tau}_Y$ and $\mathbf{K}_{ms}$ are r-dimensional vectors respectively. Also $\boldsymbol{\Lambda}$, $\boldsymbol{\Omega}$, $\boldsymbol{\Gamma}$, $\boldsymbol{\Phi}^{(t)}$, $\boldsymbol{\Phi}^{(s)}$, $\boldsymbol{\Pi}^{(t)}$, $\boldsymbol{\Pi}^{(s)}$, $\boldsymbol{\Psi}^{(t)}$ and $\boldsymbol{\Psi}^{(s)}$ are all matrices whose elements are the load transmission factors given in Appendix A with the corresponding notation. Respectively, these matrices have dimensions $N\times N$, $s\times N$, $r\times N$, $N\times s$, $N\times r$, $s\times s$, $s\times r$, $r\times s$, and $r\times r$. The N-dimensional vector $\mathbf{S}$ has components, S. The s-dimensional vector $\boldsymbol{\sigma}_Y$ has components $-\sigma_Y$ or σ_Y depending on whether the yielding is due to increasing or decreasing relative displacements of bounding fibers, i.e. $W_{j+1}-W_j$. The r-dimensional vector $\boldsymbol{\tau}_Y$ has components τ_Y or $-\tau_Y$ depending on whether shear yielding is due to positively or negatively increasing slopes of bounding fibers, i.e., $\mathrm{d}W_j/\mathrm{d}\xi+\mathrm{d}W_{j+1}/\mathrm{d}\xi$.

The actual matrix compressive stresses $\sigma_{n_j}(\xi_i)$ and shear stresses $\tau_{n_j}(\xi_j)$ in the corresponding yielded matrix elements are, respectively,

$$\sigma_{n_j}(\xi_j) = -\left\{\kappa(W_{n+1}(\xi_j)-W_n(\xi_j))+K_{mt,j}/2q\right\} \tag{68}$$

and

$$\tau_{n_k}(\xi_k) = \frac{8}{\pi}\left\{\phi\left(\frac{\mathrm{d}W_n}{\mathrm{d}\xi}+\frac{\mathrm{d}W_{n+1}}{\mathrm{d}\xi}\right)\Big|_{\xi=\xi_k}+K_{ms,k}/2q\right\}, \tag{69}$$

which show the modifications of adding, respectively, the tensile dipole force correction or shear moment dipole correction (where to calculate the associated stresses, we have divided by $2q$ or $(\pi/8)2q$, respectively). If the length $2q$ of the matrix elements is sufficiently small, the magnitudes should be very close to σ_Y or τ_Y with small fluctuations along the fiber due to the discreteness of the matrix dipole corrections and the constant shear stress corrections, as reflected in these equations. The fluctuations will indeed be small as will be seen in Section 7.

Finally the case of debonding is treated in essentially the same way, except that the residual matrix stress after debonding (possibly zero) is what appears at a matrix element that has reached the yield threshold. Matrix elements that have not reached the yield threshold (a higher value than the residual stress after debonding) may be well above the residual debond stress value.

6. Framework for investigating possible kink band initiation

We now consider the deformation behavior around an array of several fiber breaks aligned along an oblique or 'slant' plane at an angle α relative to the transverse plane perpendicular to the fiber axis, as seen in Fig. 11. Our goal is to show that a kink band initiating mechanism is possible once a small slant array of dislocations has formed due to flaws in the fibers that have resulted in initial shear failures under the original compressive strain. Indeed breaks forming many small groups of dislocations could occur randomly in the composite, but very few may have the slant alignment features necessary to grow further and trigger a kink band. The larger ϵ_c is the larger the number of initial random fiber breaks and the higher the probability that a small slant array of fiber dislocations occurs to start the kink band failure process. We do not investigate these probabilistic aspects here but merely begin with a slant array of dislocations.

6.1. Shear load induced at dislocations in a slant cluster

The angle α, which we may view as the angle of an initial slip plane for a few fibers that have failed in shear, will be varied to explore the induced bending stresses on the surviving fibers around the cluster. We will also find the particular value of α that makes those bending stresses most severe for a given axial compressive strain ϵ_c applied to the composite. We assume a simple relationship motivated by resolving shear forces $\overline{S}$ induced at the dislocations at slant angle α under the applied compressive load $\overline{P} = E_f A_f \epsilon_c$ per fiber. We choose the dimensional shear force $\overline{S}$ acting at a dislocation as

$$\overline{S} = \overline{P}\sin(\alpha). \tag{70}$$

In non-dimensional terms, this shear force is

$$S = \frac{\overline{S}}{E_f I_f/d^2} = \frac{(\pi d^2/4)\epsilon_c \sin(\alpha)}{I_f/d^2} = 16\epsilon_c \sin(\alpha), \tag{71}$$

since $I_f = \pi d^4/64$ is the fiber moment of inertia. At best, this is a crude approximation to the dislocating effects of sliding due to the compressive load, and other formulas are possible (e.g., a wedge-based formula might suggest $\tan(\alpha)$ instead of $\sin(\alpha)$), but Eq. (71) will give a reasonably good idea of the effects of changing the slant angle, α. Depending on the fiber volume fraction, V_f, we will find $\alpha \approx 25°$ so the particular choice of formula seems not to be so critical an issue. Further discussion will appear in the final section.

The main idea is that once the stage is reached where neighboring fibers are sufficiently bent to begin failing at the two locations of the peak induced bending strains, spaced a few fiber diameters apart, a catastrophic kink band will be triggered, as is seen experimentally. For very small dislocation clusters (i.e., 1, 2, or 3, say) it is also possible that only one of the four highest bending points (or even a shear load peak) will

fail a fiber thus extending the dislocation array and tending to dictate the value of the emerging angle, α. The new longer break array increases the bending stresses on the new neighbors and makes paired breaks even more likely compared to single breaks.

As mentioned, crucial to the mechanism is the possibility of yielding of the matrix in tension, compression or shear. We find that elastic analysis alone is insufficient particularly due to the existence of restraining tensile stresses in the short regions of matrix between breaks in two adjacent fibers (see Fig. 10). Matrix yielding or debonding in tension within these regions is crucial to the deformation mechanism, as is discussed in more detail in the next section.

6.2. Numerical procedure for evaluating fiber displacements and matrix stresses

Based on the theoretical solution technique developed in previous sections, we now outline our procedure for numerical implementation of the influence function, superposition technique in order to perform a parameter study of the likelihood of composite failure in compression through initiation of a kink band. A simple discretized composite lamina with four fiber breaks, is shown in Fig. 10, and though not delineated, the discrete matrix elements are identical in length and are flanked by fiber elements. For calculation purposes we use a coordinate system having nodes with spacing q. Generally, we will apply matrix tensile dipoles at the midpoints of the matrix elements (of length $2q$) and calculate matrix stresses also at those midpoints.

A significant difference between a single fiber dislocation and multiple fiber dislocations is the importance of yielding in matrix elements between adjacent broken fibers. As mentioned, between breaks in adjacent fibers (about one matrix element of length $2q$ in Fig. 10), the matrix tensile stresses will be very high and tensile yielding will occur as fibers locally move apart due to the dislocations. Shear stresses will be relatively smaller there especially for larger N as changes in slope are less. In the regions further above or below such matrix elements, i.e., outside of the adjacent break overlap zones, it is primarily the shear stresses that exceed their yielding value, as is seen in Fig. 11 where slope changes become large but relative fiber separation remains smaller. Therefore, in order to reduce computation time in repeated solution of the matrix equation Eq. (67), we mainly considered shear stress induced yielding in those outside regions and mainly tensile stress induced yielding between adjacent breaks. In the matrix bays outside the region of dislocations, as shown in Fig. 11, both types of stresses may exceed their yield limits during composite compression, but again, the tensile or compressive stresses tend to dominate because of the large changes in relative fiber displacements, and these are most important to model.

We first describe the procedure for calculating the fiber displacements and matrix bay stresses for the case of two fiber dislocations, $N = 2$, in an infinite lamina under compression. Fig. 12 illustrates this case. When the applied compressive strain ϵ_c becomes sufficiently large, the matrix stresses will be high enough to initiate plastic yielding in matrix bays 2 and -2 as shown in Fig. 12. We consider incrementally only the most heavily overloaded 'group' of matrix elements at any one time, as marked by the crossed dotted lines. In matrix bays 2 and -2, the tensile or compressive stresses at four points are calculated. If only two of the four are above the yielding stress, i.e., $|\sigma_n(\xi)|$ exceeds σ_Y, such as the upper crossed point in matrix bay 2 and lower one in matrix bay -2, we calculate the stresses at locations right next to them. If the stresses at the locations above the crossed lines in matrix bay 2 and below the crossed lines in matrix bay -2 are also beyond yielding, then we take the matrix element to be subject to yielding and construct a matrix equation (67) to calculate two matrix tension dipole weighting factors, one for each yielded element. We then iterate until equilibrium is achieved, that is, the forces or moments representing matrix element stresses match those calculated from the corresponding matrix yield stress (boundary condition) as seen on the left-hand side of Eq. (67). We also check the other two elements for stress changes.

Next, we consider matrix bays 1 and -1. We may have $|\sigma_n(\xi)|$ exceed σ_Y at two or four of the crossed points, and there may be four more potentially damaged matrix elements and tension dipole weighting

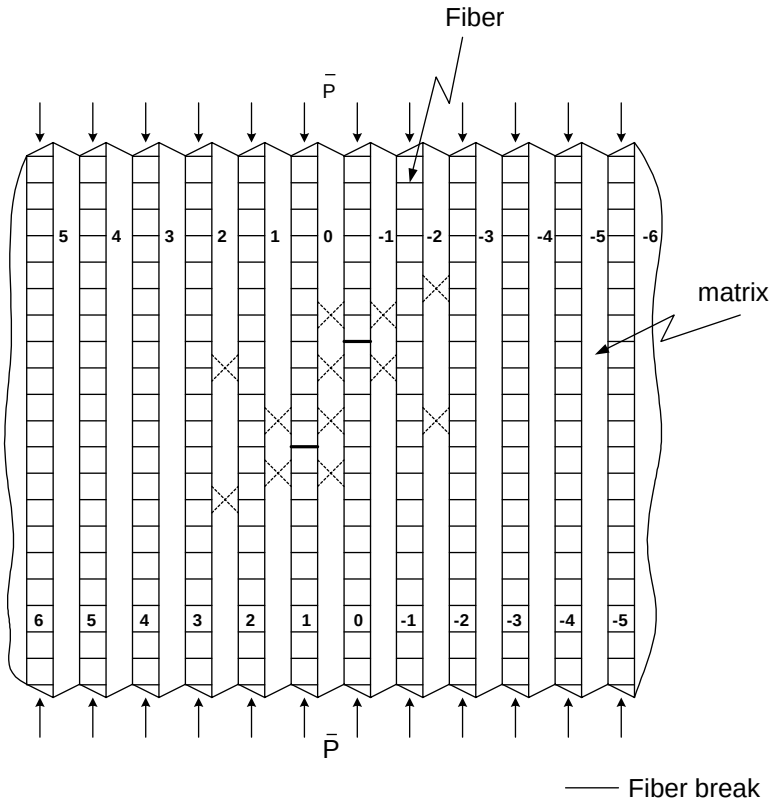

Fig. 12. Discretized two dimensional infinite lamina subjected to a remote uniform compressive load and with equal length fiber and matrix elements and two fiber breaks.

factors to consider. Again, not all four weighting factors are identical. The weighting factor for the yielded element in matrix bay 1 above the break in fiber 1 is the same as the one associated with the element in matrix bay -1 below the break in fiber 0. Similarly, the other two are identical. As above, we calculate in succession the weighting factors as warranted by the check, and iterate until equilibrium is reached.

Finally, we consider matrix bay 0 between the broken fibers. Our scheme is to calculate shear stresses at the crossed points below the break in fiber 1 and above break in fiber 0, and for $N = 2$, they happen to be the same. We also calculate the tensile stresses at those crossed points between the two breaks. If they are all above their corresponding yielding value, we then have in total 12 tensions and shear dipole-weighting factors to determine, including the two for the dislocations. These weighting factors are determined and used to recalculate the tensile or shear stresses in matrix elements adjacent to the previously yielded matrix elements to decide whether additional yielding occurs. If no adjacent matrix elements are overloaded, then the incremental process is stopped and these same 12 weighting factors are used to determine the fiber displacements everywhere. However, if $|\sigma_n(\xi)|$ or shear stress $|\tau_n(\xi)|$ in any of the neighboring matrix elements (or others) is now at above the threshold stress σ_Y or τ_Y, then corrective dipole displacement functions are required and the above calculation is repeated with a new group of adjacent elements and weighting factors, and a larger matrix equation to solve. This process is repeated incrementally until stability is finally reached and $|\sigma_n(\xi)|$ or $|\tau_n(\xi)|$ are respectively less than σ_Y or τ_Y in all non-yielding matrix elements. A typical pattern of damaged zones is shown in Fig. 13.

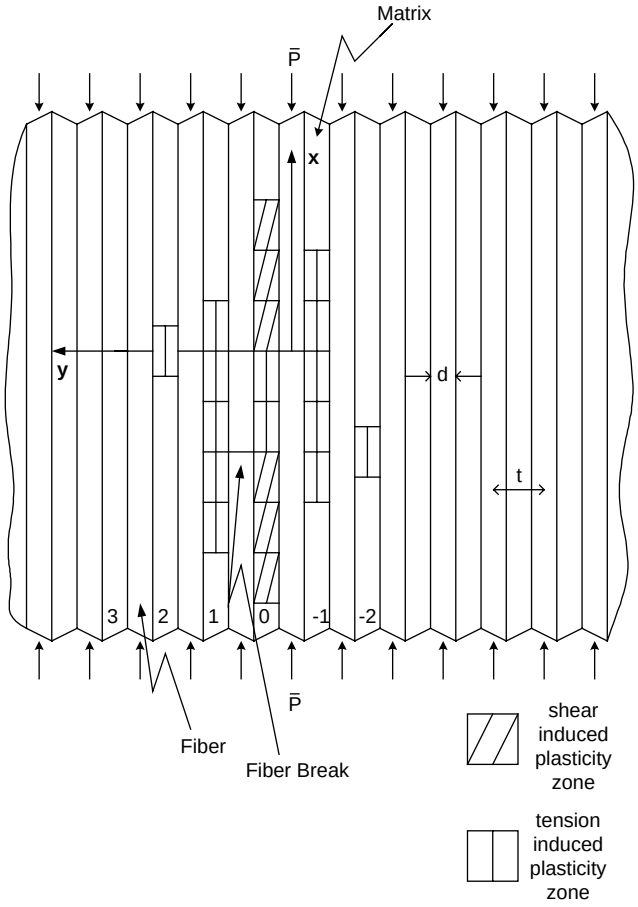

Fig. 13. Typical pattern of matrix yield zones for a pair of fiber dislocations in a two-dimensional lamina subjected to a remote axial compressive load.

7. Case studies and results

We now consider several case studies giving computed results for composite laminae whose material properties are as follows: The Young's modulus of the fiber is assumed to be

$$E_f = 300\,\mathrm{GPa}, \tag{72}$$

typical of carbon fibers, and that for the matrix taken as

$$E_m = 4.5\,\mathrm{GPa}, \tag{73}$$

a typical value for epoxy. The matrix shear modulus is taken as

$$G_m = \frac{E_m}{2(1+\nu)} = 1.61\,\mathrm{GPa}, \tag{74}$$

where we have taken $\nu = 0.4$. The matrix plastic yield stress magnitude in compression or tension is

$$\sigma_y = 45\,\mathrm{GPa}, \tag{75}$$

its yield stress in shear is

$$\tau_y = 22.5\,\text{GPa}. \tag{76}$$

Finally, the fiber failure strain in compression (occurring near the surface due to the sum of bending strain plus the far field compressive strain) is assumed to be

$$\epsilon^c_{f,\text{fail}} = 0.01. \tag{77}$$

We will consider a few different values of the fiber volume fraction taken for simplicity to be

$$V_f = d/t, \tag{78}$$

since the thickness is also d.

Throughout this section, unless indicated otherwise, the chosen slant angle, α, for the dislocation array is typically the most severe for a particular fiber volume fraction, V_f, and the material parameter choices given above. Also, we only draw the displacement or stress profiles of dislocated fibers and matrix bays on one half of the region under consideration since the other half can be obtained from symmetry or antisymmetry.

7.1. Effects of matrix plastic yielding on bending induced fiber strains

Fig. 14 shows typical displacement profiles of fibers in an $N = 2$ dislocation lamina as shown above in Fig. 13. The parameter values used for generating the plots were $V_f = 0.67$, $\epsilon_c = 0.0025$ and $\alpha = 26°$. Note

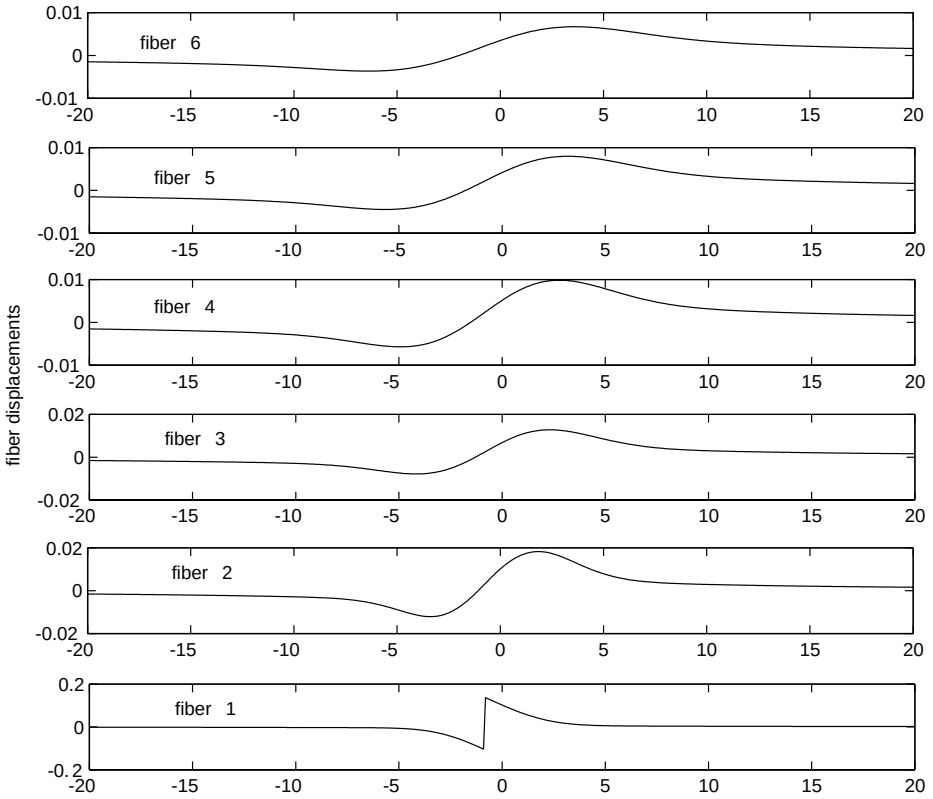

Fig. 14. Normalized displacement profiles of fibers in a lamina with $N = 2$ fiber dislocations, $V_f = 0.67$, $\epsilon_c = 0.0025$ and $\alpha = 26°$.

that the dislocation displacements are much less than one fiber diameter even in the case of substantial matrix yielding, thus revealing the destabilizing effects of relatively small local transverse fiber displacements.

Also for this two-dislocation case and $\epsilon_c = 0.0025$, Figs. 15 and 16 show the patterns of fiber bending strain (bending induced strain at the outer radius of the fiber furthest from the dislocations but not including the applied compressive strain), and matrix tensile or compressive and shear stresses, respectively. (Recall that compressive stresses are positive in sign.) Note that the displacements and compressive stresses are smooth whereas the shear stresses show slight fluctuations in the yielding zones due to the discrete nature of the shear dipole force corrections. The overall effects of the fluctuations are negligible, however.

Next we study the effect of matrix plasticity and fiber volume fraction on the local deformation and stresses as the number, N, of aligned dislocations increases. The composite compressive strain is held at $\epsilon_c = 0.002$ and the slant angle is fixed at $\alpha = 26°$. For the three fiber volume fractions, $V_f = 0.33$, 0.5 and 0.67, the maximum bending strain in the first intact fiber is shown in Figs. 17–19, respectively. For all three-fiber volume fractions, under purely elastic conditions (infinite matrix yield stresses), the maximum fiber bending-strain quickly reaches a low plateau as N increases. Once we permit plastic yielding, however, the maximum bending-strain increases much more dramatically with N. The cause of this phenomenon is that the transverse tension that develops in the matrix elements between breaks in adjacent fibers becomes relieved in the case of a plastically yielding matrix. In the purely elastic case, this tension is not relieved, and

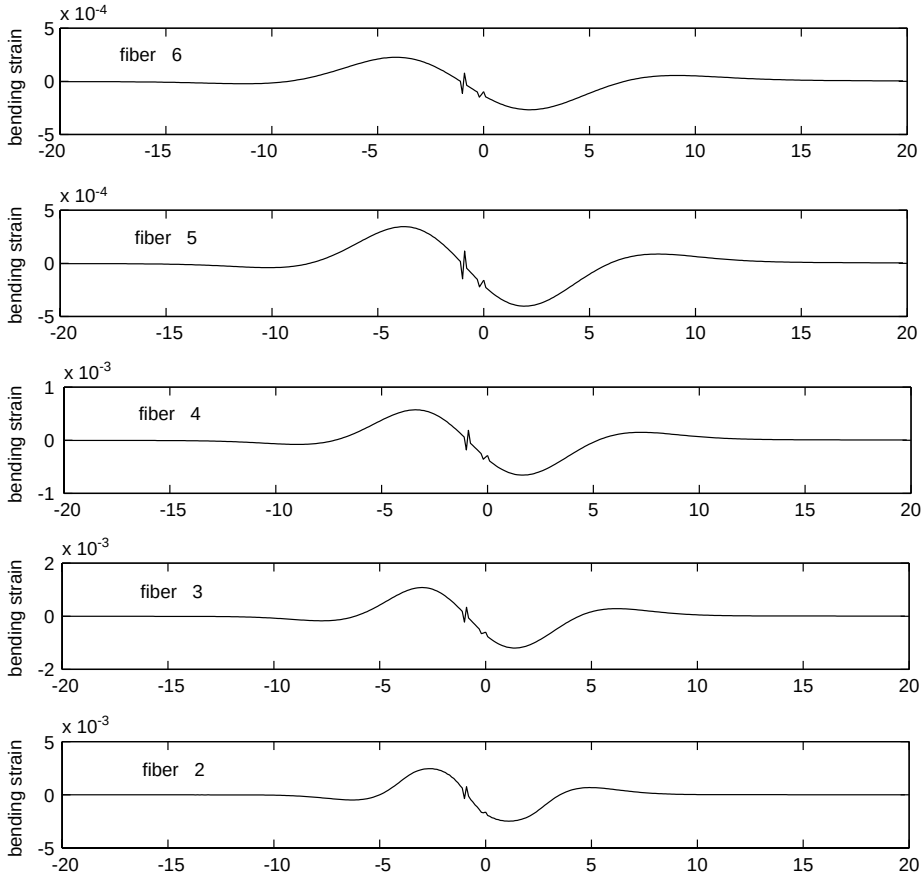

Fig. 15. Bending strain profiles of fibers in a lamina with $N = 2$ fiber dislocations, $V_f = 0.67$, $\epsilon_c = 0.0025$ and $\alpha = 26°$.

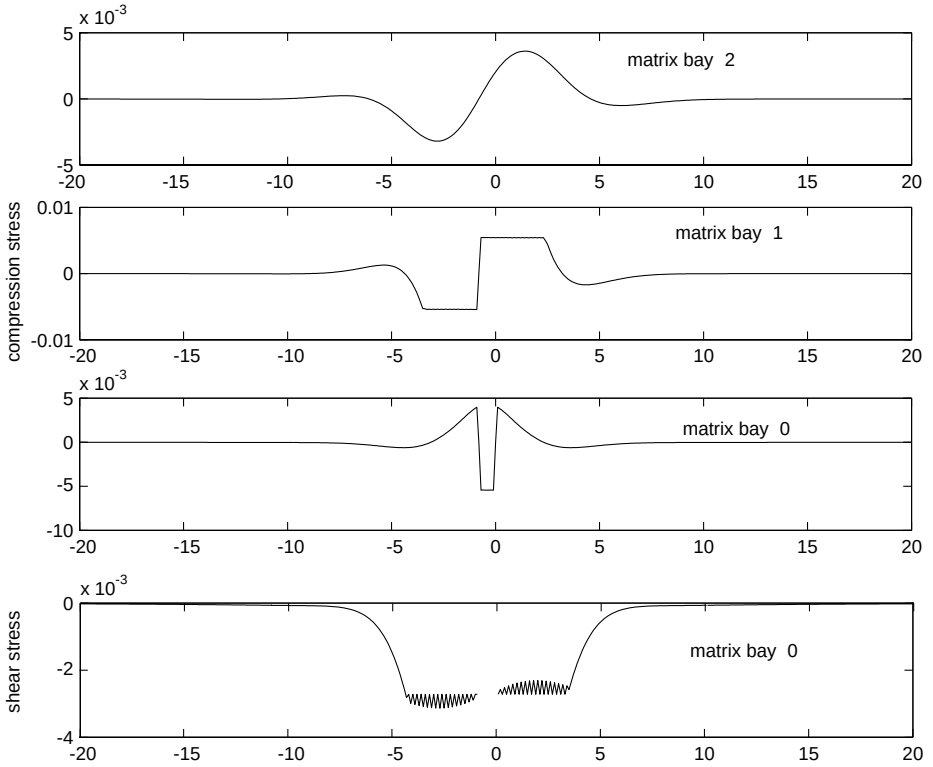

Fig. 16. Plots showing the compressive and shear stresses that develop in the matrix bays surrounding $N = 2$ fiber dislocations, where $V_f = 0.67$, $\epsilon_c = 0.0025$ and $\alpha = 26°$.

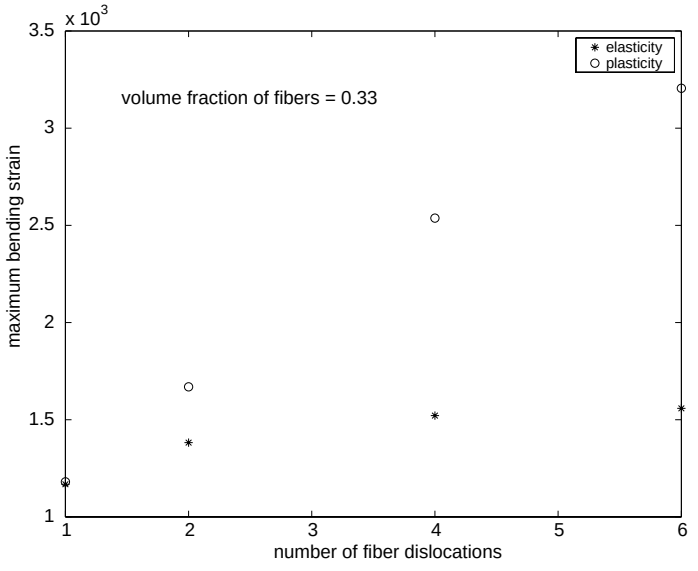

Fig. 17. Effect of allowing matrix plastic yielding on maximum fiber bending strain at $V_f = 0.33$ where $\epsilon_c = 0.002$ and $\alpha = 26°$.

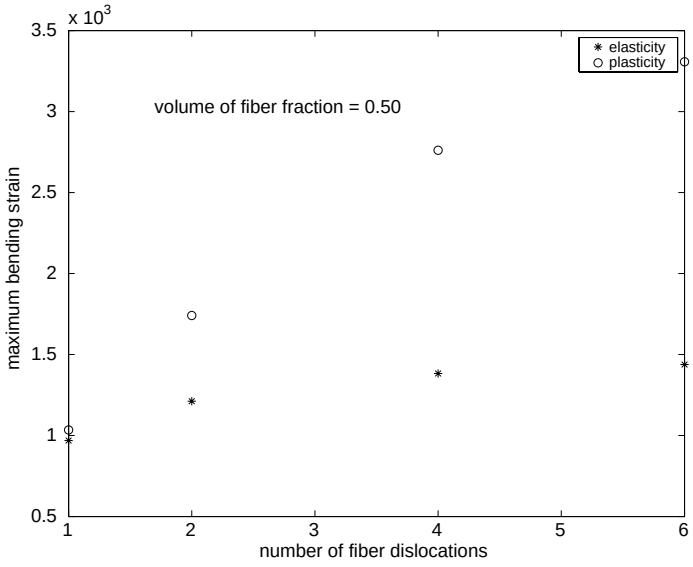

Fig. 18. Effect of allowing matrix plastic yielding on maximum fiber bending strain at $V_f = 0.50$ where $\epsilon_c = 0.002$ and $\alpha = 26°$.

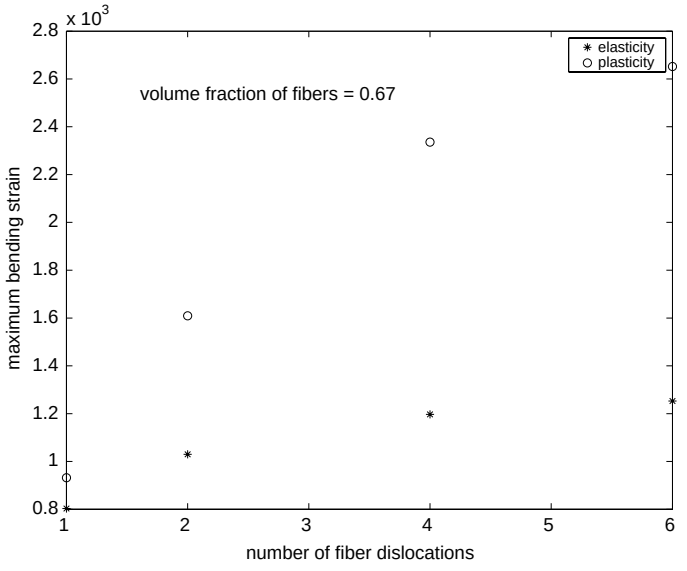

Fig. 19. Effect of allowing matrix plastic yielding on maximum fiber bending strain at $V_f = 0.67$ where $\epsilon_c = 0.002$ and $\alpha = 26°$.

thus, generates increasing opposition to further dislocation movement in each broken fiber. Note that the maximum bending strain is much larger when plastic yielding occurs. Later we consider the effects of debonding on this release of restraining tension.

Another interesting observation from Figs. 17–19 is that, in the purely elastic case with all the other parameters fixed, the maximum bending strain actually decreases as the fiber volume fraction increases.

The reason is that at higher volume fractions, the composite is stiffer and the fibers are thus less likely to deform with high curvature. In Rosen's classic model this favors the matrix shear mode for criticality over the matrix extension mode (Fig. 1) where the shear mode involves long wavelength fluctuations and the tension mode much shorter fluctuations, which are suppressed at higher V_f.

However, when we introduce matrix plastic yielding, two possible mechanisms occur: The volume fraction of fibers and size of the yield zones will work together to determine the value of maximum bending strain. Furthermore, though not illustrated, we notice that a higher fiber volume fraction results in larger lengths of the yield zones and positions between maximum bending strains in the fibers on each side. Thus, with plasticity present, the response trends differ markedly from the purely elastic case. Note that at $V_f = 0.50$, the flanking fibers unexpectedly appear to have the highest maximum bending strain, thus illustrating the complexity of the interactions.

Next we consider deformation around an $N = 4$ dislocation array as shown in Fig. 10. For a lamina with $V_f = 0.67$ and $\alpha = 26°$, Fig. 20 shows the change of bending strain of the first intact fiber next to the fiber dislocation zone as the applied strain ϵ_c is increased. The maximum bending strain indeed depends strongly on the external compressive strain. Note that the distance along the fiber between the peak locations grows with applied strain and reaches about five fiber diameters, perhaps a determining factor for the fiber fragment length, D, in the kink band. Similar results are shown in Fig. 21 for a lamina with lower $V_f = 0.50$ and dislocation line angle $\alpha = 21°$. Note that the distance along the fiber between peak strains is somewhat smaller, which is consistent with what was mentioned in the paragraph above.

We also consider the effects of the fiber dislocation zone on the bending strains and displacements of fibers further away from it. Here we choose a composite lamina with $N = 4$ dislocations under compressive strain $\epsilon_c = 0.002$ and angle $\alpha = 21°$, and in Fig. 22 we calculate the maximum bending strains (in absolute value) in the first few intact fibers on one side of the dislocation zone and under three different volume fractions of fibers, $V_f = 0.67$, 0.5 and 0.33. The effect of the fiber dislocation zone on peak bending strains appears very locally; the magnitudes die out very rapidly with distance away from the dislocated break zone.

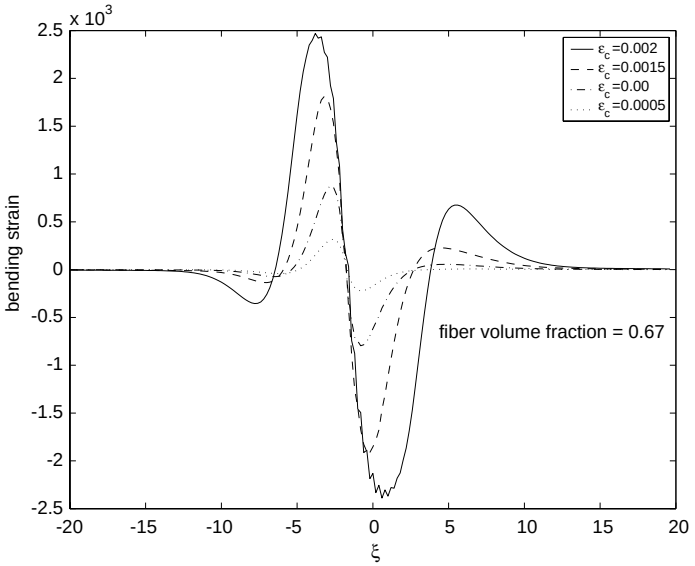

Fig. 20. Increase in bending strain in flanking fiber 3 with compressive strain ϵ_c on a lamina with $N = 4$ fiber dislocations, $V_f = 0.67$ and $\alpha = 26°$.

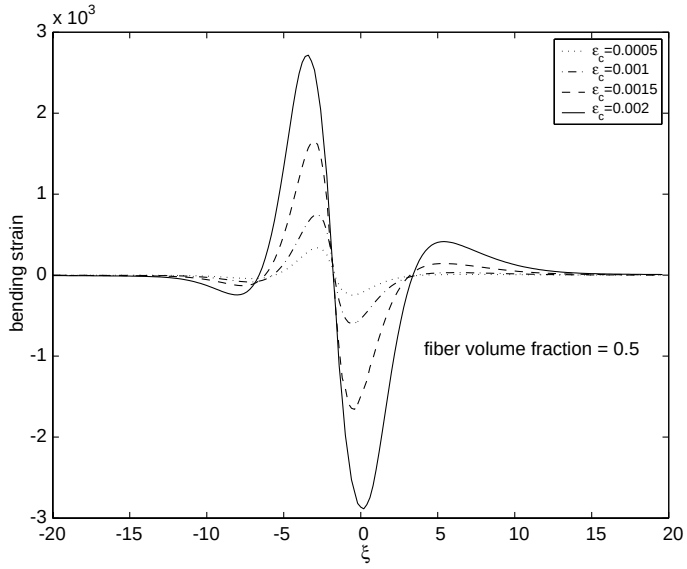

Fig. 21. Increase in bending strain of flanking fiber 3 with the compressive strain ϵ_c on a lamina with $N = 4$ fiber dislocations, $V_f = 0.50$ and $\alpha = 21°$.

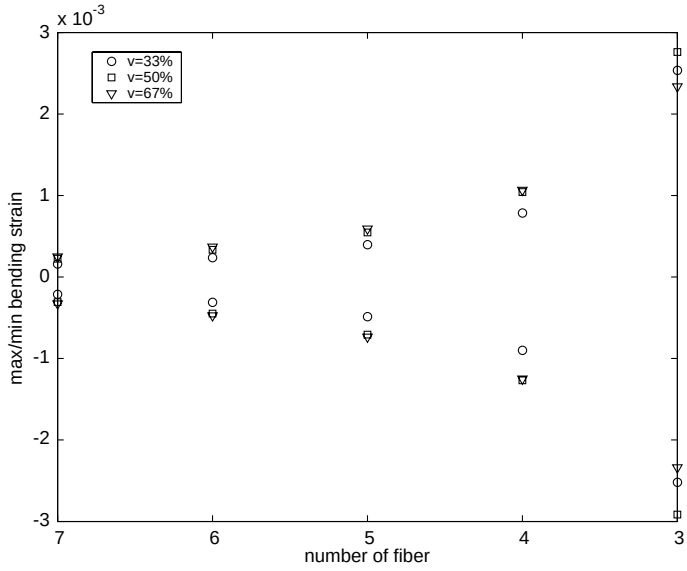

Fig. 22. Trends in peak bending-strain values in fibers further from the dislocation zone with $N = 4$ dislocations, where $V_f = 0.67$, 0.5 and 0.33 and $\alpha = 21°$.

Similarly, in Fig. 23 we calculate the maximum and minimum displacements in these intact fibers and similar trends occur.

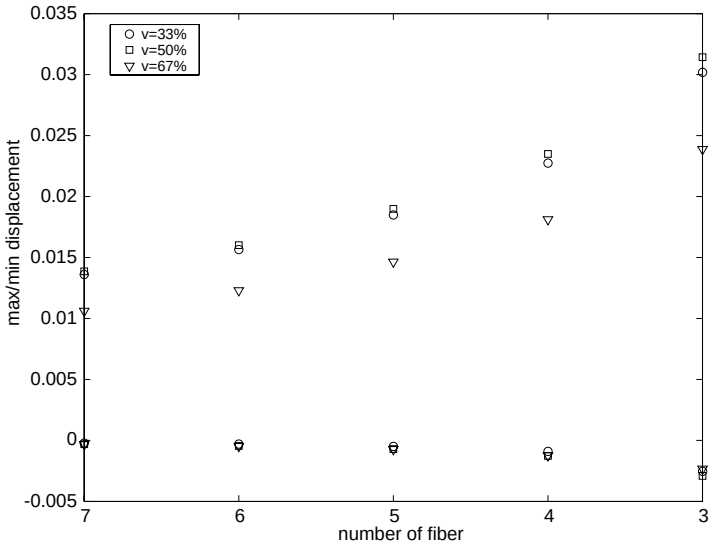

Fig. 23. Trends in peak displacement values in fibers further from the dislocation zone with $N = 4$ dislocations, where $V_f = 0.67$, 0.5 and 0.33 and $\alpha = 21°$.

7.2. Effects of matrix debonding in the overlap zones between fiber dislocations

Next we consider the effects of matrix debonding in the overlap zones between consecutive dislocated fiber breaks, where the fiber segments flanking the matrix elements are moving in opposite directions to highly stretch these matrix elements. Basically, instead of assigning a fixed stress value to the matrix elements there after yielding at $\sigma_y = 45\,\text{GPa}$, we take an after-debonding, residual stress value, $\sigma_d = 0$. There are also no yield zones beyond these regions. The main purpose is to show the importance of such debonding on fiber bending behavior during composite loading in compression. We calculate the peak bending strain values in the intact fiber adjacent to the last dislocated fiber by varying the number of dislocations and under fixed compressive strain and fiber volume fraction. This is shown in Fig. 24, which is based on a compressive strain $\epsilon_c = 0.002$, slant angle $\alpha = 26°$ and for fiber volume fraction $V_f = 0.67$. Compared to Fig. 19, which shows the purely elastic case, this matrix debonding in tension dramatically increases the fiber bending strains and so is a crucial aspect of compressive failure.

Furthermore, since severe matrix shear deformation occurs in the regions of the same matrix bays above and below the debond zones, we also allow shear-induced debonding to occur in those regions as well, where the limit strain for debonding is taken as twice the shear yielding limit to accommodate larger shear strains before debonding that can occur in shear. The trends are shown in Fig. 25 for $\epsilon_c = 0.0025$, $\alpha = 26°$ and $V_f = 0.67$. The trends are similar to the cases discussed above, except that the maximum bending strains are even larger than before (partly because ϵ_c is higher) for the case of matrix plastic yielding but no debonding.

It was found in the calculations that the distances along the fibers between the two locations of peak bending, were significantly less than occurred in the case of plastic yielding without debonding. From this observation and the bending strain values seen here compared to the case of plastic yielding, it is clear that the details of matrix yielding and debonding are very important in determining peak bending strain magnitudes and locations along the fibers for a given compressive strain, ϵ_c, on the composite.

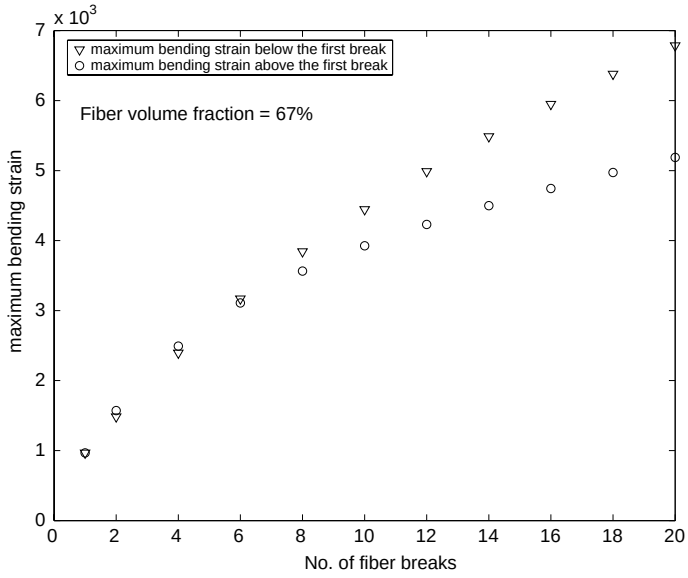

Fig. 24. Maximum bending strain in the first intact fiber versus number of dislocations under debonding in the break overlap regions and for $V_f = 0.67$, $\alpha = 26^\circ$ and $\epsilon_c = 0.002$.

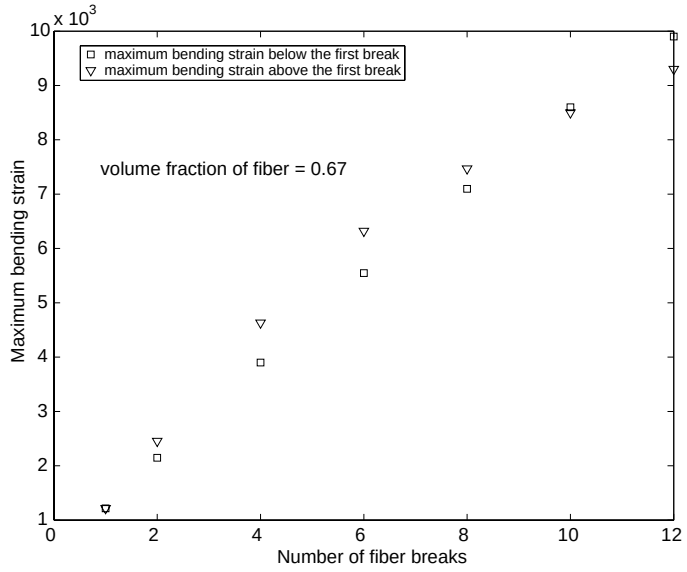

Fig. 25. Maximum bending strain in the first intact fiber at $V_f = 0.67$, $\epsilon_c = 0.0025$, and $\alpha = 26^\circ$ including debonding in both tension and shear.

Finally, specific predictions of our model are compared with values from Rosen's classic theory in Table 1, using the fiber failure strain given by Eq. (77) and where bending and applied compressive strains are superimposed. Note that in Rosen's shear mode for compressive failure the failure strain of the fiber

Table 1
Comparison of predicted compressive failure strains of the composite for current model versus those of the classic Rosen model in the shear mode $\epsilon_{c,cr} = \frac{G_m/E_f}{(1-V_f)V_f}$, where $V_f = 0.67$ and for the fiber itself $\epsilon^c_{f,\text{fail}} = 0.01$

No. of fiber dislocations	2	4	6	8
Rosen's shear mode ($\epsilon_{c,cr}$)	0.0242	0.0242	0.0242	0.0242
Current model ($\epsilon_{c,cr}$)	<0.0052	<0.004	<0.0031	<0.0026

($\epsilon^c_{f,\text{fail}} = 0.01$) has no role. The results show that our model produces predictions much lower than those of Rosen bringing them to a level more in line with experiments.

8. Discussion and conclusions

We have considered a mechanism for compressive failure based on transverse displacements of fibers near N dislocations due to fiber shear failures at multiple weak flaws and by chance aligned in an array at a slant angle, α. We have shown that such deformation leads to large bending strains in the fibers flanking the N dislocation array at pairs of points along each fiber that could trigger a kink band, and that these bending strains increase rapidly with N. Furthermore, the optimal slant angle and distances between peak bending strain points appear to depend strongly on the fiber volume fraction, and fiber and matrix mechanical properties, especially the matrix plastic yield and debonding thresholds. Further work, however, would be necessary to simulate the actual evolution of a kink band and determine parameters as in Fig. 2.

The model has several potential shortcomings that should be mentioned: First, it is reasonable to question whether the shear failure angles of the fibers should necessarily match the angle, α, of the slant array that is optimal for bending failures in flanking fibers. While there is some leeway, shear failure angles that are too small will not give rise initially to significant values of the fiber shear loads, $\overline{S}$, at the dislocations, whereas if such angles are too large compared to α, interference from fiber end wedge overlaps may prevent significant dislocation motion. This is clearly an issue worthy of more detailed study.

Second the model is a 2D model whereas real composites have 3D features. This would obviously change and complicate the system of fourth-order differential equations. Unlike the case of tensile failure, however, where damage development tends to become axisymmetric (often modelled using penny shaped cracks, for instance), failure in compression retains directional features involving some slanted plane of collapse. Thus, apart from more complicating statistical fiber failure effects, a 3D square array of fibers might fail much like the 2D array here and indeed the failure load may be lower because there are more choices available for damage development.

Perhaps more important than the above is that, unlike in the work of Garland et al. (2001), our model does not treat the longitudinal fiber displacements at fiber shear (or crushing) failures, an extreme example of which is shown in Fig. 3. In tensile failure, opening displacements can be one to several fiber diameters, thus causing substantial tensile load concentrations on fibers next to small arrays of contiguous fiber breaks. In compression, however, such load concentration is subdued by resistance to interpenetration that would be due to bulk compressive resistance from the debris. In other words, the debris must occupy space and there is nowhere initially to easily accommodate it.

Also, our model for the shear force $\overline{S}$ at fiber dislocations, given by Eq. (71), does not allow for local drops in the fiber loads to below $\overline{P}$ as a result of interpenetration displacements, nor to compressive fiber overloads above $\overline{P}$ on flanking fibers. These do, however, have a tendency to cancel insofar as their effects on the maximum strains in flanking fibers due to superimposed bending (reduced) and axial compression (increased).

It should also be noted that whereas, matrix yielding and debonding enhances bending failure due to lateral dislocation movement, it reduces fiber overloads in tensile failure and is also likely to do the same in simple axial compression on neighboring fibers. Furthermore, as Table 1 shows, for a given number, N, of fiber breaks, the bending strains plus compressive strains added together greatly reduce the compressive strength of the composite compared to strength reductions in tension, which can be shown to be much milder in Beyerlein and Phoenix (1996).

While there is good reason to believe that the dislocation driven mechanism in the present paper can be the dominant one, a more elaborate model should be developed, which couples the fourth-order differential equation system here for transverse displacements with the second-order system in Garland et al. (2001) for longitudinal displacements. One could then determine how the two effects may couple in compressive failure, and uncover details of the mechanism of kink band formation and propagation.

Acknowledgments

This work was supported under a NASA University Institute, the Institute for Future Space Transport (IFST), which is monitored through NASA Glenn Research Center. We would like to thank Deborah Schorr for allowing us to use Fig. 3 from her Cornell senior thesis (Schorr, 2001).

Appendix A. Load transmission factors

The nine load transmission factors used in Section 5 are given by the following mathematical formulas, where the functions $A(\theta)$, $B(\theta)$, $C(\theta)$ and $D(\theta)$ are given, respectively, by Eqs. (33)–(36). The values are obtained by numerical integration for all grid separation distances $\xi_k-\xi_i$ and n_k-n_i of interest to exhibit displacement variation between fibers. These values are then stored and recalled for use in the matrix equation (67).

For transmission from a dislocation to a dislocation we have

$$\begin{aligned}
\Lambda_{k,i}=&\frac{1}{2\pi}\int_0^{\vartheta}\frac{B(\theta)\mathrm{e}^{-B(\theta)|\xi_k-\xi_i|}-A(\theta)\mathrm{e}^{-A(\theta)|\xi_k-\xi_i|}}{B^2(\theta)-A^2(\theta)}A^2(\theta)B^2(\theta)(\cos[(n_k-n_i)\theta])\,\mathrm{d}\theta\\
&+\frac{1}{4\pi}\int_{\vartheta}^{\pi}\mathrm{e}^{-C(\theta)|\xi_k-\xi_i|}\left(\frac{\cos(D(\theta)|\xi_k-\xi_i|)}{C(\theta)}-\frac{\sin(D(\theta)|\xi_k-\xi_i|)}{D(\theta)}\right)[C^2(\theta)+D^2(\theta)]^2(\cos[(n_k-n_i)\theta])\,\mathrm{d}\theta\\
&-\phi\left\{\frac{1}{2\pi}\int_0^{\vartheta}\frac{A(\theta)\mathrm{e}^{-B(\theta)|\xi_k-\xi_i|}-B(\theta)\mathrm{e}^{-A(\theta)|\xi_k-\xi_i|}}{B^2(\theta)-A^2(\theta)}A(\theta)B(\theta)(\cos[(n_k-n_i+1)\theta]\right.\\
&\quad+2\cos[(n_k-n_i)\theta]+\cos[(n_k-n_i-1)\theta])\,\mathrm{d}\theta\\
&\quad-\frac{1}{4\pi}\int_{\vartheta}^{\pi}\mathrm{e}^{-C(\theta)|\xi_k-\xi_i|}\left(\frac{\cos(D(\theta)|\xi_k-\xi_i|)}{C(\theta)}+\frac{\sin(D(\theta)|\xi_k-\xi_i|)}{D(\theta)}\right)[C^2(\theta)+D^2(\theta)](\cos[(n_k-n_i+1)\theta]\\
&\quad\left.+2\cos[(n_k-n_i)\theta]+\cos[(n_k-n_i-1)\theta])\,\mathrm{d}\theta\right\}\\
&+16\epsilon_c\left\{\frac{1}{2\pi}\int_0^{\vartheta}\frac{A(\theta)\mathrm{e}^{-B(\theta)|\xi_k-\xi_i|}-B(\theta)\mathrm{e}^{-A(\theta)|\xi_k-\xi_i|}}{B^2(\theta)-A^2(\theta)}A(\theta)B(\theta)(\cos[(n_k-n_i)\theta])\,\mathrm{d}\theta\right.\\
&\quad\left.-\frac{1}{4\pi}\int_{\vartheta}^{\pi}\mathrm{e}^{-C(\theta)|\xi_k-\xi_i|}\left(\frac{\cos(D(\theta)|\xi_k-\xi_i|)}{C(\theta)}+\frac{\sin(D(\theta)|\xi_k-\xi_i|)}{D(\theta)}\right)[C^2(\theta)+D^2(\theta)](\cos[(n_k-n_i)\theta])\mathrm{d}\theta\right\}.
\end{aligned}\tag{A.1}$$

For a dislocation to matrix element in tension or compression we have

$$\begin{aligned}\Omega_{k,i} = 2q\kappa\,\mathrm{sign}(\xi_k-\xi_i)\Bigg\{&\frac{1}{2\pi}\int_0^{\vartheta}\frac{\mathrm{e}^{-A(\theta)|\xi_k-\xi_i|}B^2(\theta)-\mathrm{e}^{-B(\theta)|\xi_k-\xi_i|}A^2(\theta)}{B^2(\theta)-A^2(\theta)}\\&\times\left(\cos[(n_k-n_i+1)\theta]-\cos[(n_k-n_i)\theta]\right)\mathrm{d}\theta\\&+\frac{1}{2\pi}\int_{\vartheta}^{\pi}\mathrm{e}^{-C(\theta)|\xi_k-\xi_i|}\left(\cos[D(\theta)|\xi_k-\xi_i|]+\frac{C^2(\theta)-D^2(\theta)}{2C(\theta)D(\theta)}\sin[D(\theta)|\xi_k-\xi_i|]\right)\\&\times\left(\cos[(n_k-n_i+1)\theta]-\cos[(n_k-n_i)\theta]\right)\mathrm{d}\theta\Bigg\}.\end{aligned}\tag{A.2}$$

For a dislocation to matrix element in shear we have

$$\begin{aligned}\Gamma_{k,i} = 2q\left(\frac{\pi}{8}\right)\left(\frac{8\phi}{\pi}\right)\Bigg\{&\frac{1}{2\pi}\int_0^{\vartheta}\frac{\mathrm{e}^{-B(\theta)|\xi_k-\xi_i|}A(\theta)-\mathrm{e}^{-A(\theta)|\xi_k-\xi_i|}B(\theta)}{B^2(\theta)-A^2(\theta)}\\&\times A(\theta)B(\theta)\left(\cos[(n_k-n_i+1)\theta]+\cos[(n_k-n_i)\theta]\right)\mathrm{d}\theta\\&-\frac{1}{4\pi}\int_{\vartheta}^{\pi}\mathrm{e}^{-C(\theta)|\xi_k-\xi_i|}\left(\frac{\cos[D(\theta)|\xi_k-\xi_i|]}{C(\theta)}+\frac{\sin[D(\theta)|\xi_k-\xi_i|]}{D(\theta)}\right)\\&\times\left(C^2(\theta)+D^2(\theta)\right)\left(\cos[(n_k-n_i+1)\theta]+\cos[(n_k-n_i)\theta]\right)\mathrm{d}\theta\Bigg\}.\end{aligned}\tag{A.3}$$

For a matrix element tension dipole to a dislocation we have

$$\begin{aligned}\Phi^{(t)}_{j,k} = -\mathrm{sign}(\xi_j-\xi_k)\Bigg\{&\frac{1}{2\pi}\int_0^{\vartheta}\frac{A^2(\theta)\mathrm{e}^{-A(\theta)|\xi_j-\xi_k|}-B^2(\theta)\mathrm{e}^{-B(\theta)|\xi_j-\xi_k|}}{A^2(\theta)-B^2(\theta)}\\&\times\left(\cos[(n_j-n_k)\theta]-\cos[(n_j-n_k-1)\theta]\right)\mathrm{d}\theta\\&-\frac{1}{4\pi}\int_{\vartheta}^{\pi}\mathrm{e}^{-C(\theta)|\xi_j-\xi_k|}\left(\cos[(n_j-n_k)\theta]-\cos[(n_j-n_k-1)\theta]\right)\\&\times\frac{(C^2(\theta)-D^2(\theta))\sin[D(\theta)|\xi_j-\xi_k|]-2C(\theta)D(\theta)\cos[D(\theta)|\xi_j-\xi_k|]}{C(\theta)D(\theta)}\,\mathrm{d}\theta\Bigg\}\\&+\phi\,\mathrm{sign}(\xi_j-\xi_k)\Bigg\{\frac{1}{2\pi}\int_0^{\vartheta}\frac{\mathrm{e}^{-B(\theta)|\xi_j-\xi_k|}-\mathrm{e}^{-A(\theta)|\xi_j-\xi_k|}}{B^2(\theta)-A^2(\theta)}\\&\times\left(\cos[(n_j-n_k+1)\theta]+\cos[(n_j-n_k)\theta]-\cos[(n_j-n_k-1)\theta]-\cos[(n_j-n_k-2)\theta]\right)\mathrm{d}\theta\\&+\frac{1}{4\pi}\int_{\vartheta}^{\pi}\mathrm{e}^{-C(\theta)|\xi_k-\xi_j|}\frac{\sin[D(\theta)|\xi_k-\xi_j|]}{C(\theta)D(\theta)}\\&\times\left(\cos[(n_j-n_k+1)\theta]+\cos[(n_j-n_k)\theta]-\cos[(n_j-n_k-1)\theta]-\cos[(n_j-n_k-2)\theta]\right)\mathrm{d}\theta\Bigg\}\\&-16\epsilon_c\,\mathrm{sign}(\xi_j-\xi_k)\Bigg\{\frac{1}{2\pi}\int_0^{\vartheta}\frac{\mathrm{e}^{-B(\theta)|\xi_j-\xi_k|}-\mathrm{e}^{-A(\theta)|\xi_j-\xi_k|}}{B^2(\theta)-A^2(\theta)}\left(\cos[(n_j-n_k)\theta]-\cos[(n_j-n_k-1)\theta]\right)\mathrm{d}\theta\\&-\frac{1}{4\pi}\int_{\vartheta}^{\pi}\mathrm{e}^{-C(\theta)|\xi_k-\xi_j|}\frac{\sin[D(\theta)|\xi_k-\xi_j|]}{C(\theta)D(\theta)}\left(\cos[(n_j-n_k)\theta]-\cos[(n_j-n_k-1)\theta]\right)\mathrm{d}\theta\Bigg\}.\end{aligned}\tag{A.4}$$

For a matrix element tension dipole to a matrix element in tension we have

$$\begin{aligned}\Pi^{(t)}_{l,k} = -2q\kappa\Bigg\{&\frac{1}{2\pi}\int_0^{\vartheta}\frac{B(\theta)\mathrm{e}^{-A(\theta)|\xi_l-\xi_k|}-A(\theta)\mathrm{e}^{-B(\theta)|\xi_l-\xi_k|}}{A(\theta)B(\theta)(B^2(\theta)-A^2(\theta))}\\&\times(\cos[(n_l-n_k+1)\theta]-2\cos[(n_l-n_k)\theta]+\cos[(n_l-n_k-1)\theta])\,\mathrm{d}\theta\\&+\frac{1}{4\pi}\int_{\vartheta}^{\pi}\frac{C(\theta)\sin(D(\theta)|\xi_l-\xi_k|)+D(\theta)\cos(D(\theta)|\xi_l-\xi_k|)}{[C^2(\theta)+D^2(\theta)]C(\theta)D(\theta)}\\&\times\mathrm{e}^{-C(\theta)|\xi_l-\xi_k|}(\cos[(n_l-n_k+1)\theta]-2\cos[(n_l-n_k)\theta]+\cos[(n_l-n_k-1)\theta])\,\mathrm{d}\theta\Bigg\}.\end{aligned}\tag{A.5}$$

For a matrix element tension dipole to a matrix element in shear we have

$$\begin{aligned}\Psi^{(t)}_{l,k} = -2q\left(\frac{\pi}{8}\right)\left(\frac{8\phi}{\pi}\right)\mathrm{sign}(\xi_l-\xi_k)\Bigg\{&\frac{1}{2\pi}\int_0^{\vartheta}\frac{\mathrm{e}^{-A(\theta)|\xi_l-\xi_k|}-\mathrm{e}^{-B(\theta)|\xi_l-\xi_k|}}{A^2(\theta)-B^2(\theta)}\\&\times(\cos[(n_l-n_k+1)\theta]-\cos[(n_l-n_k-1)\theta])\,\mathrm{d}\theta\\&-\frac{1}{4\pi}\int_{\vartheta}^{\pi}\frac{\sin[D(\theta)|\xi_l-\xi_k|]}{C(\theta)D(\theta)}\mathrm{e}^{-C(\theta)|\xi_l-\xi_k|}(\cos[(n_l-n_k+1)\theta]-\cos[(n_l-n_k-1)\theta])\,\mathrm{d}\theta\Bigg\}.\end{aligned}\tag{A.6}$$

For a matrix element shear (moment) dipole to a dislocation

$$\begin{aligned}\Phi^{(s)}_{j,l} = &\frac{1}{2\pi}\int_0^{\vartheta}\frac{A^3(\theta)\mathrm{e}^{-A(\theta)|\xi_j-\xi_l|}-B^3(\theta)\mathrm{e}^{-B(\theta)|\xi_j-\xi_l|}}{A^2(\theta)-B^2(\theta)}\big(\cos[(n_j-n_l)\theta]+\cos[(n_j-n_l-1)\theta]\big)\,\mathrm{d}\theta\\&-\frac{1}{4\pi}\Bigg\{\int_{\vartheta}^{\pi}\frac{\mathrm{e}^{-C(\theta)|\xi_j-\xi_l|}}{C(\theta)D(\theta)}\big[(C^3(\theta)-3C(\theta)D^2(\theta))\sin[D(\theta)|\xi_j-\xi_l|]\\&+(D^3(\theta)-3D(\theta)C^2(\theta))\cos[D(\theta)|\xi_j-\xi_l|]\big]\big(\cos[(n_j-n_l)\theta]+\cos[(n_j-n_l-1)\theta]\big)\,\mathrm{d}\theta\Bigg\}\\&+\phi\Bigg\{\frac{1}{2\pi}\int_0^{\vartheta}\left(\frac{B(\theta)\mathrm{e}^{-B(\theta)|\xi_j-\xi_l|}-A(\theta)\mathrm{e}^{-A(\theta)|\xi_j-\xi_l|}}{A^2(\theta)-B^2(\theta)}\right)\big(\cos((n_j-n_l+1)\theta)\\&+3\cos((n_j-n_l)\theta)+3\cos((n_j-n_l-1)\theta)+\cos((n_j-n_l-2)\theta)\big)\,\mathrm{d}\theta\\&+\frac{1}{4\pi}\int_{\vartheta}^{\pi}\mathrm{e}^{-C(\theta)|\xi_j-\xi_l|}\left(\frac{C(\theta)\sin(D(\theta)|\xi_j-\xi_l|)-D(\theta)\cos(D(\theta)|\xi_j-\xi_l|)}{C(\theta)D(\theta)}\right)\\&\times\big(\cos((n_j-n_l+1)\theta)+3\cos((n_j-n_l)\theta)+3\cos((n_j-n_l-1)\theta)+\cos((n_j-n_l-2)\theta)\big)\,\mathrm{d}\theta\Bigg\}\\&-16\epsilon_c\Bigg\{\frac{1}{2\pi}\int_0^{\vartheta}\left(\frac{B(\theta)\mathrm{e}^{-B(\theta)|\xi_j-\xi_l|}-A(\theta)\mathrm{e}^{-A(\theta)|\xi_j-\xi_l|}}{A^2(\theta)-B^2(\theta)}\right)\big(\cos[(n_j-n_l)\theta]+\cos[(n_j-n_l-1)\theta]\big)\,\mathrm{d}\theta\\&+\frac{1}{4\pi}\int_{\vartheta}^{\pi}\mathrm{e}^{-C(\theta)|\xi_j-\xi_l|}\left(\frac{C(\theta)\sin(D(\theta)|\xi_j-\xi_l|)-D(\theta)\cos(D(\theta)|\xi_j-\xi_l|)}{C(\theta)D(\theta)}\right)\\&\times\big(\cos[(n_j-n_l-1)\theta]+\cos[(n_j-n_l)\theta]\big)\,\mathrm{d}\theta\Bigg\}.\end{aligned}\tag{A.7}$$

For a matrix element shear (moment) dipole to matrix element in tension we have

$$\begin{aligned}\Pi^{(s)}_{m,r} = 2q\kappa\,\mathrm{sign}(\xi_m-\xi_r)\Bigg\{&\frac{1}{2\pi}\int_0^{\vartheta}\frac{\mathrm{e}^{-B(\theta)|\xi_m-\xi_r|}-\mathrm{e}^{-A(\theta)|\xi_m-\xi_r|}}{A^2(\theta)-B^2(\theta)}(\cos[(n_m-n_r+1)\theta]-\cos[(n_m-n_r-1)\theta])\,\mathrm{d}\theta\\&+\frac{1}{4\pi}\int_{\vartheta}^{\pi}\mathrm{e}^{-C(\theta)|\xi_m-\xi_r|}\left(\frac{\sin(D(\theta)|\xi_m-\xi_r|)}{C(\theta)D(\theta)}\right)(\cos[(n_m-n_r+1)\theta]-\cos[(n_m-n_r-1)\theta])\,\mathrm{d}\theta\Bigg\}.\end{aligned}\tag{A.8}$$

Finally, for a matrix element shear (moment) dipole to matrix element in shear we have

$$\begin{aligned}\Psi^{(s)}_{g,k} = 2q\left(\frac{\pi}{8}\right)\left(\frac{8\phi}{\pi}\right)\Bigg\{&\frac{1}{2\pi}\int_0^{\vartheta}\frac{A(\theta)\mathrm{e}^{-A(\theta)|\xi_g-\xi_k|}-B(\theta)\mathrm{e}^{-B(\theta)|\xi_g-\xi_k|}}{A^2(\theta)-B^2(\theta)}\big(\cos[(n_g-n_k+1)\theta]\\&+2\cos[(n_g-n_k)\theta]+\cos[(n_g-n_k-1)\theta]\big)\,\mathrm{d}\theta\\&-\frac{1}{4\pi}\int_{\vartheta}^{\pi}\mathrm{e}^{-C(\theta)|\xi_g-\xi_k|}\frac{C(\theta)\sin(D(\theta)|\xi_g-\xi_k|)-D(\theta)\cos(D(\theta)|\xi_g-\xi_k|)}{C(\theta)D(\theta)}\\&\times\big(\cos[(n_g-n_k+1)\theta]+2\cos[(n_g-n_k)\theta]+\cos[(n_g-n_k-1)\theta]\big)\,\mathrm{d}\theta\Bigg\}.\end{aligned}\tag{A.9}$$

References

Argon, A.S., 1972. Fracture of composites. In: Treatise on Material Science and Technology, Vol. 1. Academic Press, New York, pp. 79–114.

Berbinau, P., Soutis, C., Guz, I.A., 1999. Compressive failure of 0° unidirectional carbon-fibre-reinforced plastics (cfrp) laminates laminates by fibre microbuckling. Compos. Sci. Technol. 59, 1451–1455.

Beyerlein, I.J., Phoenix, S.L., 1996. Stress concentrations around multiple fiber breaks in an elastic matrix with local yielding or debonding using quadratic influence superposition. J. Mech. Phys. Solids 44, 1997–2039.

Boll, D.J., Jensen, R.M., Cordner, L., Bascom, W.D., 1990. Compressive behavior of single carbon filaments embedded in an epoxy polymer. J. Compos. Mater. 24, 208–219.

Budiansky, B., 1983. Micromechanics. Comput. Struct. 16, 3–12.

Budiansky, B., Fleck, N.A., 1993. Compressive failure of fibre composites. J. Mech. Phys. Solids 41, 183–211.

Chaudhuri, R.A., Xie, M., Garala, H., 1996. Stress singularity due to kink band weakening a unidirectional composite under compression. J. Compos. Mater. 30, 672–691.

Evans, A.G., Adler, W.F., 1978. Kinking as a mode of structural fiber degradation in carbon fiber composites. Acta Metall. 26, 725–738.

Fleck, N.A., Deng, L., Budiansky, B., 1995. Prediction of kink band width in compressed fiber composites. ASME J. Appl. Mech. 62, 329–337.

Garland, B., Beyerlein, I.J., Schadler, L.S., 2001. Kink band initiation by damage zones in fibrous composites. Compos. Sci. Technol. 61, 2461–2480.

Goutianos, S., Peijs, T., Galiotis, C., 2002. Mechanisms of stress transfer and interface integrity in carbon/epoxy composites under compression loading part I: Experimental investigation. Int. J. Solids Struct. 39, 3217–3231.

Goutianos, S., Peijs, T., Galiotis, C., 2003. Mechanisms of stress transfer and interface integrity in carbon/epoxy composites under compression loading part II: Numerical approach. Int. J. Solids Struct. 40, 5521–5538.

Greszczuk, L.B., 1982. On failure modes of unidirectional composites under compressive loading. In: Proc. 2nd USA-USSR Sump. on Fracture of Composite Materials. Martinus Nijhoff, The Hague, NL, pp. 231–244.

Ha, J.B., Nairn, J.A., 1992. Compression failure mechanisms of single-ply, unidirectional, carbon-fiber composites. SAMPE Quart. 23, 29–36.

Hahn, H.T., Sohi, M.M., 1986. Buckling of a fiber bundle embedded in epoxy. Comp. Sci. Technol. 27, 25–41.

Hahn, H.T., Williams, J.G., 1986. Compression failure mechanisms in unidirectional composites. In: Composite Materials Testing and DesignSTP 893. ASTM, Philadelphia, PA, pp. 115–139.

Hawthorne, H.M., Teghtsoonian, E., 1975. Axial compression fracture in carbon fibres. J. Mater. Sci. 10, 41–51.

Lee, S.H., Waas, A.M., 1999. Compressive response and failure of fiber reinforced unidirectional composites. Int. J. Fract. 100, 275–306.

Narayanan, S., Schadler, L.S., 1999. Mechanism of kink-band formation in graphite/epoxy composites: a micromechanical experimental study. Compos. Sci. Technol. 59, 2201–2213.

Oshawa, T., Miwa, M., Kawade, M., Tsushima, E., 1990. Axial compressive strength of carbon fiber. J. Appl. Poly. Sci. 39, 1733–1743.

Rosen, B.W., 1965. Mechanics of composites strengthening. In: Fiber Composite Materials. American Society for Metals, Metals Park, OH, pp. 37–75.

Schorr, D., 2001. Compressive failure mechanisms of single filament carbon fiber reinforced composites. Senior Thesis, Department of Materials Science and Engineering, Cornell University.

Schultheisz, C.R., Waas, A.M., 1996. Compressive failure of composites, part I: Testing and micromechanical theories. Prog. Aerosp. Sci. 32, 1–42.

Shioya, M., Nakatani, M., 2000. Compressive strength of single carbon fibres and composite strands. Comp. Sci. Technol. 60, 219–229.
Steif, P.S., 1990a. A model for kinking in fiber composites—I. Fiber breakage via microbuckling. Int. J. Solids Struct. 26, 549–561.
Steif, P.S., 1990b. A model for kinking in fiber composites—II. Kink band formation. Int. J. Solids Struct. 26, 563–569.
Vogler, T.J., Kyriakides, S., 1999a. On the axial propagation of kink bands in fiber composites: Part I experiments. Int. J. Solids Struct. 36, 557–574.
Vogler, T.J., Kyriakides, S., 1999b. On the axial propagation of kink bands in fiber composites: Part II analysis. Int. J. Solids Struct. 36, 575–595.
Waas, A.M., Schultheisz, C.R., 1996. Compressive failure of composites, part II: Experimental studies. Prog. Aerosp. Sci. 32, 43–78.
Waas, A.M., Babcock, C.D., Knauss, W.G., 1990. A mechanical model for elastic fiber microbuckling. J. Appl. Mech. 57, 138–149.
Yerramalli, C.S., Waas, A.M., 2003. A failure criterion for fiber reinforced polymer composites under combined compression-torsion loading. Int. J. Solids Struct. 40, 1139–1164.
Yerramalli, C.S., Waas, A.M., 2004a. The effect of fiber diameter on the compressive strength of composites—a 3d finite element based study. Comput. Model. Eng. Sci. 6, 1–16.
Yerramalli, C.S., Waas, A.M., 2004b. A non-dimensional number to classify composite compressive failure. J. Appl. Mech. 71, 402–408.